Monthly Notices
of the
ROYAL ASTRONOMICAL SOCIETY

MNRAS **465,** 4703–4722 (2017)
Advance Access publication 2016 November 29

doi:10.1093/mnras/stw3055

The universal rotation curve of dwarf disc galaxies

E. V. Karukes[1,2,3]★ and P. Salucci[1,2]★

[1]*SISSA International School for Advanced Studies, Via Bonomea 265, I-34136 Trieste, Italy*
[2]*INFN, Sezione di Trieste, Via Valerio 2, I-34127 Trieste, Italy*
[3]*ICTP South American Institute for Fundamental Research, Instituto de Física Teórica – Universidade Estadual Paulista (UNESP), Rua Dr Bento Teobaldo Ferraz 271, 01140-070 São Paulo, Brazil*

Accepted 2016 November 22. Received 2016 November 4; in original form 2016 July 20

ABSTRACT

We use the concept of the spiral rotation curves universality to investigate the luminous and dark matter properties of the dwarf disc galaxies in the local volume (size ∼11 Mpc). Our sample includes 36 objects with rotation curves carefully selected from the literature. We find that, despite the large variations of our sample in luminosities (∼2 of dex), the rotation curves in specifically normalized units, look all alike and lead to the lower mass version of the universal rotation curve of spiral galaxies found in Persic et al. We mass model the double normalized universal rotation curve $V(R/R_{\rm opt})/V_{\rm opt}$ of dwarf disc galaxies: the results show that these systems are totally dominated by dark matter whose density shows a core size between 2 and 3 stellar disc scalelengths. Similar to galaxies of different Hubble types and luminosities, the core radius r_0 and the central density ρ_0 of the dark matter halo of these objects are related by $\rho_0 r_0 \sim 100\,{\rm M}_\odot\,{\rm pc}^{-2}$. The structural properties of the dark and luminous matter emerge very well correlated. In addition, to describe these relations, we need to introduce a new parameter, measuring the compactness of light distribution of a (dwarf) disc galaxy. These structural properties also indicate that there is no evidence of abrupt decline at the faint end of the baryonic to halo mass relation. Finally, we find that the distributions of the stellar disc and its dark matter halo are closely related.

Key words: galaxies: dwarf – galaxies: formation – galaxies: haloes – galaxies: kinematics and dynamics – dark matter.

1 INTRODUCTION

It is widely believed that only 15 per cent of the total matter in the Universe is in the form of ordinary baryonic matter. Instead the other 85 per cent is provided by dark matter (DM), which is detectable, up to now, only through its gravitational influence on luminous matter. The paradigm is that DM is made by massive gravitationally interacting elementary particles with extremely weak, if not null interaction via other forces (e.g. White & Negroponte 1982; Jungman, Kamionkowski & Griest 1996). In this framework, the well-known (Λ) cold dark matter (CDM) scenario, successfully describing the large structure of the Universe, has emerged (Kolb & Turner 1990): accurate *N*-body simulations have found that the DM density profile of the virialized structures such as galactic haloes is universal and well described by the Navarro–Frenk–White profile (hereafter NFW; Navarro, Frenk & White 1996b).

However, at the galactic scales, this scenario has significant challenges.

First, the apparent mismatch between the number of the detected satellites around the Milky Way and the predictions of the corresponding simulations, known as the 'missing satellite problem' (Klypin et al. 1999; Moore et al. 1999), which also occurs in the field galaxies (Zavala et al. 2009; Papastergis et al. 2011; Klypin et al. 2015). This discrepancy widens up when the masses of the detected satellites are compared to those of the predicted subhaloes (i.e. 'too big to fail problem'; see Boylan-Kolchin, Bullock & Kaplinghat 2012; Ferrero et al. 2012; Garrison-Kimmel et al. 2014; Papastergis et al. 2015).

Furthermore, there is the 'core–cusp' controversy: the inner DM density profiles of galaxies generally appear to be cored, and not cuspy as predicted in the simplest (Λ)CDM scenario (e.g. Salucci 2001; de Blok & Bosma 2002; Bosma 2004; Gentile et al. 2004, 2005, 2007; Simon et al. 2005; Del Popolo & Kroupa 2009; Donato et al. 2009; Oh et al. 2011; Weinberg et al. 2015, to name few).

These apparent discrepancies between the observations and the predictions of the DM-only simulations suggest to either abandon the (Λ)CDM scenario in favour of the others (e.g. self-interacting DM,Vogelsberger et al. 2014; Elbert et al. 2015 or warm DM, de Vega & Sanchez 2013; de Vega et al. 2013; de Vega, Salucci &

★ E-mail: ekarukes@sissa.it (EVK); salucci@sissa.it (PS)

Sanchez 2014; Lovell et al. 2014) or upgrade the role of baryonic physics in the galaxy formation process. The latter can be done including strong gas outflows, triggered by stellar and/or AGN feedback that are thought to strongly modify the original (Λ)CDM halo profiles out to a distance as large as the size of the stellar disc (e.g. Navarro, Eke & Frenk 1996a; Read & Gilmore 2005; Mashchenko, Couchman & Wadsley 2006; Pontzen & Governato 2012, 2014; Di Cintio et al. 2014).

Although these issues are present in galaxies of any luminosity; however, in low-luminosity systems they emerge more clearly and appear much more difficult to be resolved within the (Λ)CDM scenario. Thus, galaxies with *I*-band absolute magnitude $M_I \gtrsim -17$ play a pivotal role in that, observationally, these objects are DM dominated at all radii. Moreover in the (Λ)CDM scenario, they may be related to the building blocks of more massive galaxies. In light of this, the importance of dwarf spheroidal galaxies in various DM issues is well known (see, e.g. Gilmore et al. 2007). However, down to $M_I \sim -11$ there is no shortage of rotationally supported late-type systems, although a systematic investigation is lacking. These rotationally supported systems have a rather simple kinematics suitable for investigating the properties of their DM content.

In normal spirals, one efficient way to represent and model their rotation curves (RCs) comes from the concept of a universal rotation curve (URC). Let us stress that the concept of universality in RCs does not mean that all of them have a unique profile, but that all the RCs of 10^9 local spirals (within $z \simeq 0.1$) can be described by a same function of radius, modulated by few free parameters. They depend on the galaxy's global properties, namely magnitude (or luminosity/mass) and a characteristic radius of the luminous matter[1] so that: $V(R) = V(R, L, R_{\rm opt})$.

This concept, implicit in Rubin et al. (1985), pioneered by Persic & Salucci (1991), set by Persic et al. (1996, PSS, Paper I) and extended to large galactocentric radii by Salucci et al. (2007) has provided us the mass distribution of (normal) disc galaxies in the magnitude range $-23.5 \lesssim M_I \lesssim -17$.[2] This curve $V(R, L, R_{\rm opt})$, therefore, encodes all the main structural properties of the dark and luminous matter of every spiral (PSS; Yegorova & Salucci 2007). In this paper, we work out to extend the RCs universality down to low-mass systems and then, to use it to investigate the DM distribution in dwarf disc (dd) galaxies.

Noticeably, for this population of galaxies the approach of stacking the available kinematics is very useful. In fact, presently, for disc systems with the optical velocity $V_{\rm opt} \lesssim 61\,{\rm km\,s^{-1}}$, some kinematical data have become available (galaxies of higher velocities are investigated in the PSS sample). However, there are not enough individual *high-quality high-resolution extended* RCs to provide us with a solid knowledge of their internal distribution of mass. Instead, we will prove that the 36 selected in literature *good-quality good-resolution reasonably extended* RCs (see below for these definitions), once co-added, provide us with a reliable kinematics yielding to their mass distribution.

In this work, we construct a sample of dds from the local volume catalogue (LVC) (Karachentsev, Makarov & Kaisina 2013, hereafter K13), which is ∼70 per cent complete down to $M_B \approx -14$ and out to 11 Mpc, with the distances of galaxies obtained by means of primary distance indicators.

Using LVC, we go more than 3 mag fainter with respect to the sample of spirals of PSS. Moreover, the characteristics of the LVC guarantee us against several luminosity biases that may affect such faint objects. The total number of objects in this catalogue is ∼900 of which ∼180 are dwarf spheroidal galaxies, ∼500 are dd galaxies and the rest are ellipticals and spirals.

All our galaxies are low-mass bulgeless systems in which rotation, corrected for the pressure support, totally balances the gravitational force. Morphologically, they can be divided into two main types: gas-rich dwarfs that are forming stars at a relatively low rate, named irregulars (Irrs) and starbursting dwarfs that are forming stars at an unusually high rate, named blue compact dwarfs (BCD). The dwarf Irr galaxies are named 'irregulars' due to the fact that they usually do not have a defined disc shape and the star formation is not organized in spiral arms. However, some gas-rich dwarfs can have diffuse, broken spiral arms and be classified as late-type spirals (Sd) or as Magellanic spirals (Sm). The starbursting dwarfs are classified as BCD due to their blue colours, high surface brightness and low luminosities. Note that it is not always easy to distinguish among these types since the galaxies we are considering often share the same parameters space for many structural properties (e.g. Kormendy 1985; Binggeli 1994; Tolstoy, Hill & Tosi 2009).

In this paper, we neglect the morphology of the baryonic components as long as their stellar disc component follows a radially exponential surface density profile; the identifiers of a galaxy are $V_{\rm opt}$, its disc length-scale $R_{\rm D}$ and its *K*-band magnitude M_K that can be substituted by its disc mass. We refer to these systems of any morphologies and $M_K \gtrsim -18$ as dds.

In order to compare galaxy luminosities in different bands, we write down the dd relations between the magnitudes in different bands $\langle B - K\rangle \simeq 2.35$ (Jarrett et al. 2003) and $\langle B - I\rangle \simeq 1.35$ (Fukugita, Shimasaku & Ichikawa 1995).

The plan of this paper is as follows: in Section 2, we describe the sample that we are going to use; in Section 3, we introduce the analysis used to build the synthetic RC; in Section 4, we do the mass modelling of the synthetic RC; in Section 5, we denormalize the results of the mass modelling in order to describe individually our sample of galaxies and then we define their scaling relations; in Section 6, we discuss our main results.

2 THE SAMPLE

We construct our dd galaxy sample out of the LVC (K13) by adopting the following four selection criteria:

(1) we include disc galaxies with the optical velocity less than ∼61 km s^{-1} (disc systems with larger velocity amplitude are studied in PSS);

(2) the RCs extend to at least 3.2 disc scalelengths.[3] However, we allowed ourselves to extrapolate modestly the RCs of UGC1501, UGC8837, UGC5272 and IC10 due to their smoothness;

(3) the RCs are symmetric, smooth and with an average internal uncertainty less than 20 per cent;

(4) the galaxy disc length-scale $R_{\rm D}$ and the inclination function $1/\sin i$ are known within 20 per cent uncertainty.

[1] i.e. optical radius $R_{\rm opt}$ defined as the radius encompassing 83 per cent of the total luminosity.

[2] Extensions of the URC to other Hubble types are investigated in Salucci & Persic (1997) and Noordermeer et al. (2007).

[3] $R_{\rm opt} \simeq 3.2 R_{\rm D}$

Table 1. Sample of dd galaxies. Columns: (1) galaxy name; (2) galaxy distance; (3) RC source; (4) exponential scalelength of a galaxy stellar disc; (5) disc scalelength source; (6) rotation velocity at the optical radius; (7) absolute magnitude in K band.

Name	D	RCs refs	$R_{\rm D}$	$R_{\rm D}$ refs	$V_{\rm opt}$	M_K
–	(Mpc)	–	(kpc)	–	(km s^{-1})	(mag)
(1)	(2)	(3)	(4)	(5)	(6)	(7)
		Hα; H I				
UGC1281	4.94	1; 2	0.99	a	53.8	−17.97
UGC1501	4.97	1; –	1.32	a	50.2	−18.19
UGC5427	7.11	1; –	0.38	e	54.0	−17.06
UGC7559	4.88	–; 2,3	0.88	b	37.4	−16.91
UGC8837	7.21	–; 2	1.55	b	47.6	−18.25
UGC7047	4.31	–; 2,4	0.57	c	37.0	−17.41
UGC5272	7.11	–; 2	1.28	b	55.0	−16.81
DDO52	10.28	–; 3	1.30	b	60.0	−17.69
DDO101	16.1	–; 3	0.94	b	58.8	−19.01
DDO154	4.04	–; 3	0.75	b	38.0	−15.70
DDO168	4.33	–; 3	0.83	b	60.0	−17.07
Haro29	5.68	–; 3,4	0.28	b	32.6	−16.26
Haro36	8.9	–; 3	0.97	h	56.5	−17.63
IC10	0.66	–; 3	0.38	b	41.0	−17.59
NGC2366	3.19	–; 3,4	1.28	b	55.0	−18.38
WLM	0.97	–; 3	0.55	b	33.0	−15.93
UGC7603	8.4	–; 2	1.11	2	60.3	−19.07
UGC7861	7.9	–; 5	0.62	i	61.0	−19.74
NGC1560	3.45	–; 6	1.10	6	56.1	−18.43
DDO125	2.74	1; 2	0.49	c	17.0	−16.96
UGC5423	8.71	1; 12	0.52	d	39.5	−17.71
UGC7866	4.57	–; 2	0.54	2	28.7	−17.18
DDO43	5.73	–; 3	0.57	b	35.3	−15.72
IC1613	0.73	–; 3	0.60	b	19.0	−16.89
UGC4483	3.21	–; 4	0.16	f	20.8	−14.20
KK246	7.83	–; 9	0.58	9	34.6	−16.17
NGC6822	0.5	–; 10	0.56	b	35.0	−17.50
UGC7916	9.1	–; 2	1.63	h	37.0	−16.22
UGC5918	7.45	–; 2	1.23	2	45.0	−17.50
AndIV	7.17	–; 11	0.48	11	32.2	−14.78
UGC7232	2.82	–; 2	0.21	f	37.0	−16.46
DDO133	4.85	–; 3	0.9	g	42.4	−17.31
UGC8508	2.69	1; 3	0.28	j	25.5	−15.58
UGC2455	7.8	–; 2	1.06	h	47.0	−19.91
NGC3741	3.03	–; 7	0.18	c	23.6	−15.15
UGC11583	5.89	–; 8	0.17	8	52.2	−16.55

Notes. RC and $R_{\rm D}$ references: Moiseev (2014) – 1, Swaters et al. (2009) – 2, Oh et al. (2015) – 3, Lelli, Verheijen & Fraternali (2014) – 4, Epinat et al. (2008) – 5, Gentile et al. (2010) – 6, Gentile et al. (2007) – 7, Begum & Chengalur (2004) – 8, Gentile et al. (2012) – 9, Weldrake, de Blok & Walter (2003) – 10, Karachentsev et al. (2016) – 11, Oh et al. 2011 – 12, van Zee (2001) – a, Hunter & Elmegreen (2004) – b, Sharina et al. (2008) – c, Parodi, Barazza & Binggeli (2002) – d, Simard et al. (2011) – e, Martin (1998) – f, Hunter et al. (2011) – g, Herrmann, Hunter & Elmegreen (2013) – h, Yoshino & Yamauchi (2015) – i, Hunter et al. (2012) – j. Distance D and absolute magnitude in K-band M_K are taken from Karachentsev et al. (2013).

It is worth noticing that for an RC to fulfil criteria (2)–(4), it is sufficient to qualify it for the co-addition procedure but not necessarily this is the case for the individual modelling.

The kinematical data used in our analysis are H I and Hα RCs available in the literature (see Table 1), which are corrected for inclination and instrumental effects. Furthermore, circular velocities of low-mass galaxies, with $V_{\rm max} \lesssim 50$ km s^{-1}, require to be checked for the pressure support correction, this can be done using the so-called asymmetric drift correction (Dalcanton & Stilp 2010). Therefore, most of the RCs in our sample either have the asymmetric drift correction applied (the ones taken from Gentile et al. 2010, 2012; Oh et al. 2011, 2015; Lelli et al. 2014) or pressure support has been determined and is too small to affect the RC (the ones taken from Weldrake et al. 2003; Swaters et al. 2009; Karachentsev et al. 2016). Despite that we leave three galaxies (UGC1501, UGC5427 and UGC7861) for which circular velocities were not corrected. In view of their $V_{\rm max}$ are larger than 50 km s^{-1}, therefore the effect should be minor. In the innermost regions of galaxies, when available, we use also Hα data not corrected for the asymmetric drift since such term is negligible as it was pointed out by e.g. Swaters et al. (2009) and Lelli et al. (2012).

We stress that the above selection process has left out few objects whose RCs are sometimes considered in literature, e.g. the RC of DDO 70 described by Oh et al. (2015) has failed our criteria (3) because of its abnormal shape. Our approach stands firmly that, in order to provide us with proper and correct information about a galaxy dark and luminous mass distribution, the relative kinematical and the photometric data must reach a well-defined level of quality, otherwise they will be confusing rather than enlightening the issue.

Therefore, we ended with the final sample of 36 galaxies spanning the magnitude and disc radii intervals, $-19 \lesssim M_I \lesssim -13$, 0.18 kpc $\lesssim R_{\rm D} \lesssim$ 1.63 kpc and the optical velocities 17 km s^{-1} $\lesssim V_{\rm opt} \lesssim$ 61 km s^{-1} (see Table 1, the references for H I and Hα RCs of our sample are also given in the table and the individual RCs are plotted in Fig. A1 of Appendix A).

The average optical radius $\langle R_{\rm opt} \rangle$ and the log average optical velocity $\langle V_{\rm opt} \rangle$ of our sample are 2.5 kpc, 40.0 km s^{-1}, respectively, (these values will be specifically needed in Section 5). For a comparison, the galaxy sample of PSS spans the magnitude interval $-23.5 \lesssim M_I \lesssim -17$, the optical disc radii 6.4 kpc $\lesssim R_{\rm D} \lesssim$ 96 kpc, and the optical velocities between 70 km s^{-1} $\lesssim V_{\rm opt} \lesssim$ 300 km s^{-1}. Therefore, our sample will extend the URC of PSS by two orders of magnitude down in galaxy luminosity. However, let us stress that, differently from PSS, we are going to construct only one luminosity bin. This is, first, due to the fact that the amount of galaxies in our sample is small compare to that of PSS and, secondly, due to the fact that, after the normalizing procedure, they all converge to the same RC profile independently of the galaxy luminosity (see next section).

3 THE URC OF DWARF DISCS

First, we plot the RCs of galaxies in our sample expressed in physical units in log–log scales (see the left-hand panel of Fig. 1). We realize, even at a first glance, that, contrary to the RCs of normal spirals (see, e.g. Yegorova & Salucci 2007, PSS), each dd galaxy has an RC with a very different profile, as it has also been noticed by Oman et al. (2015). In other words, all curves are rising with radius but at a very different place.

Surprisingly, the origin of such diversity is closely linked with the very large scatter that the dds show in the relationship between the optical radius $R_{\rm opt}$ and the luminosity L_K, which is shown in Fig. 2. In our sample, the relation still holds but the scatter remarkably increased, while in normal spirals luminosities and disc sizes are very well correlated.

Thus, in dd galaxies, by following the analogous PSS procedure, we are going to derive a universal profile of their RCs. As an initial step of the co-addition procedure (see PSS for details), each of the 36 $V(R)$ has been normalized to its own optical radius $R_{\rm opt}$ and to its optical velocity $V_{\rm opt}$ obtained by RC data interpolation. We then

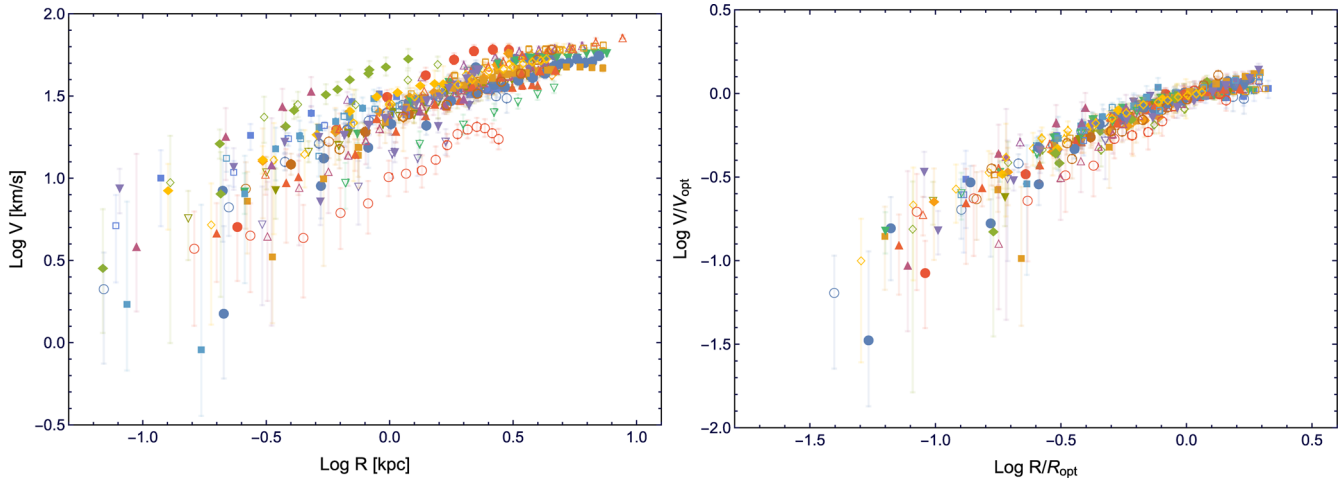

Figure 1. Individual RCs. Left-hand panel: in physical units. Right-hand panel: after double normalization on R_{opt} and V_{opt}.

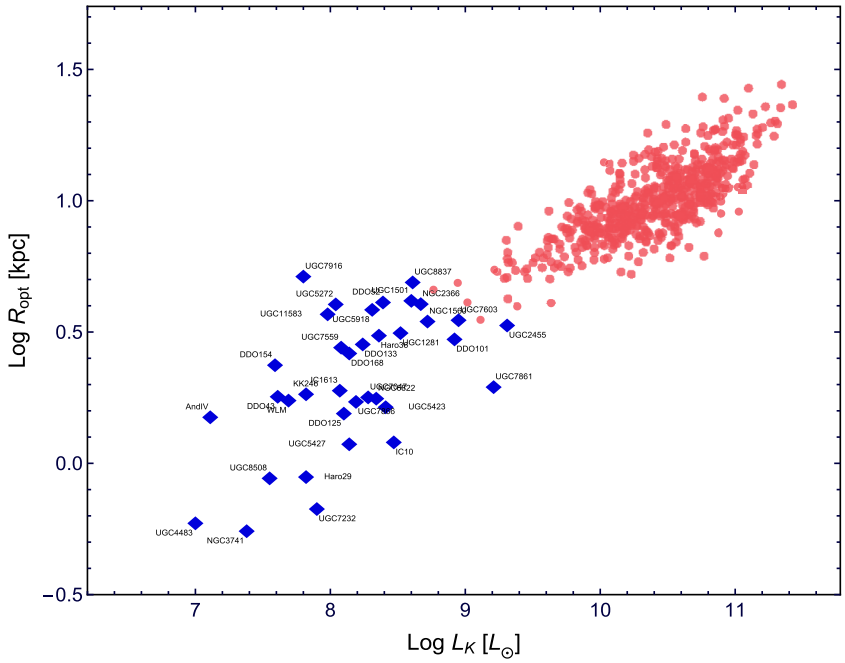

Figure 2. The optical radius versus the total luminosity. Red circles indicate the normal spiral galaxies from the sample of PSS and blue diamonds are the dwarf galaxies of this work.

derive the quantity $V(R/R_{opt})/V(R_{opt})$. This double normalization eliminates most of the small-scale individualities of the RCs.[4] In the right-hand panel of Fig. 1, you can see that all the double normalized RCs of our sample converge to a profile very similar to that of the least luminous normal spirals (red joined circles of Fig. B1).

Note that this effect is not new: in Verheijen & de Blok (1999) and Salucci & Persic (1997, see also McGaugh 2014), the variety of RCs shapes in physical units between high surface brightness galaxies and LSB objects of similar maximum velocities were eliminated by normalizing $V(R)$ on the corresponding disc scalelengths. Related to this issue, there are also several studies that have analysed quantitatively the shapes of the RCs of different morphological types of galaxies (see, e.g. Swaters et al. 2009; Lelli et al. 2014; Erroz-Ferrer et al. 2016).

Next step is to obtain the corresponding raw synthetic RC. For this purpose, the double normalized velocity data are co-added as follows: we set 14 radial bins in the position r_i[5] given by the vertical dashed grey lines in Fig. 3 and reported in Table 2. Each bin is equally divided in two, we adopt that every RC can contribute to each of the 28 semibins only with one data point. For an RC with more data points concurring to the same semibin, these are averaged accordingly. The last bin is set at $r_i = 1.9$ due to the lack of outer data.

Since a galaxy cannot contribute more than twice to every bin i, each of them, centred at r_i (see Table 2) and with boundaries shown in Fig. 3, has a number N_i data (see Table 2), which runs from a

[4] The double normalization refers to both quantities plotted on the X-axis and Y-axis of Fig. 3.

[5] Calculated as a mean value in a bin.

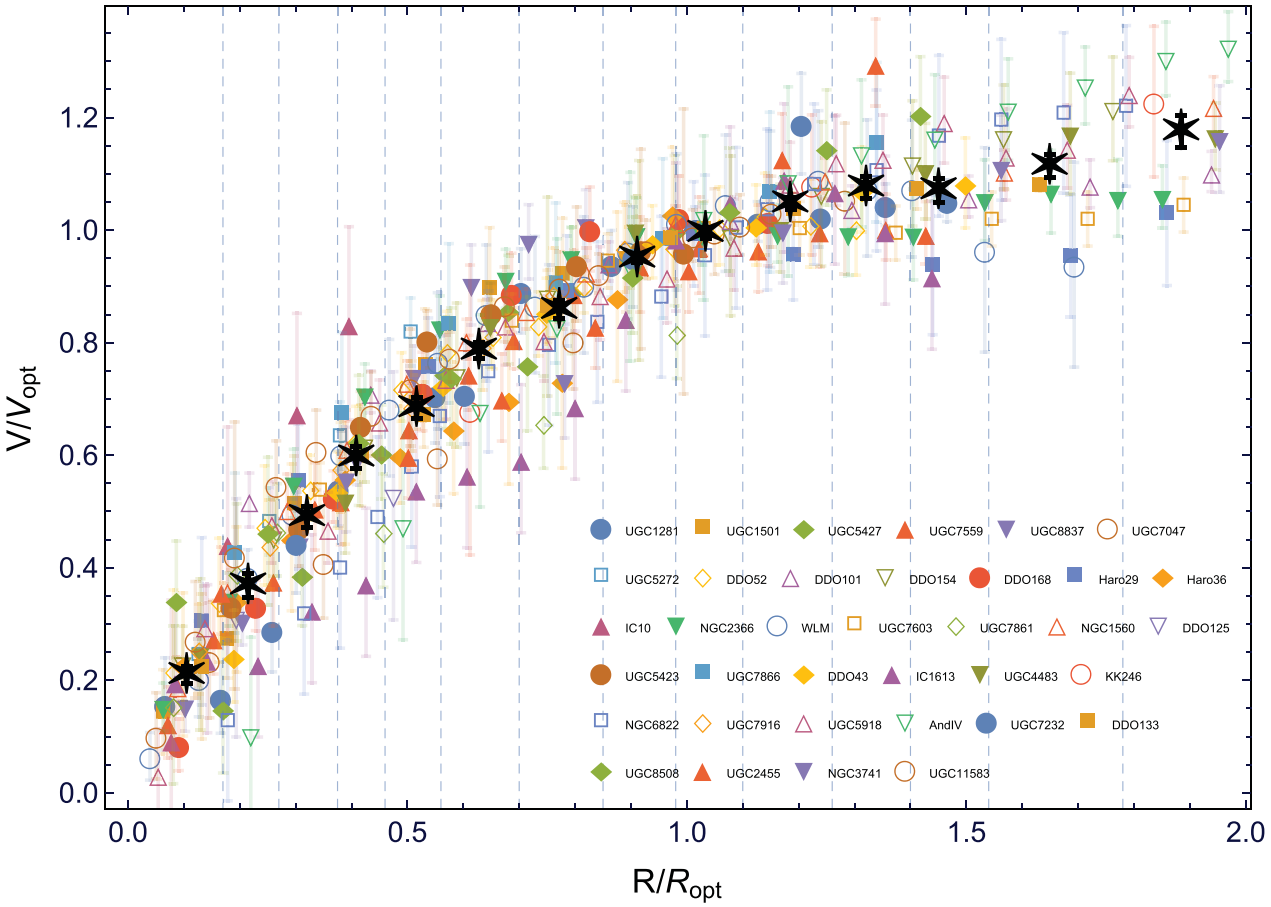

Figure 3. Individual RCs normalized to R_{opt} and V_{opt}. Black stars indicate the synthetic RC. Bins are shown as vertical dashed grey lines.

Table 2. Data in the radial bins. Columns: (1) bin number; (2) number of data points; (3) the central value of a bin; (4) the average co-added weighted normalized rotation velocity; (5) rms on the average co-added rotation velocity; (6) denormalized on $\langle R_{opt}\rangle$ values of radii, kpc; (7) denormalized on $\langle V_{opt}\rangle$ values of velocities, km s^{-1}; (8) rms on the denormalized rotation velocity.

i (1)	N (2)	r_i (3)	v_i (4)	dv_i (5)	R_i (6)	V_i (7)	dV_i (8)
1	31	0.11	0.21	0.015	0.27	8.38	0.60
2	30	0.22	0.37	0.021	0.54	14.57	0.83
3	21	0.32	0.49	0.019	0.81	19.61	075
4	26	0.41	0.60	0.019	1.03	23. 90	0.78
5	25	0.52	0.68	0.018	1.30	27.36	0.74
6	33	0.63	0.78	0.014	1.58	31.41	0.57
7	34	0.77	0.86	0.016	1.94	34.31	0.65
8	28	0.91	0.95	0.009	2.29	37.88	0.35
9	25	1.03	0.99	0.009	2.60	39.64	0.38
10	28	1.18	1.05	0.010	2.97	41.79	0.39
11	18	1.32	1.07	0.018	3.31	42.97	0.72
12	17	1.45	1.07	0.020	3.65	42.68	0.78
13	20	1.65	1.12	0.020	4.13	44.70	0.80
14	14	1.88	1.20	0.030	4.73	47.83	1.18

maximum of 68 and a minimum that we have set to be 14. Then, from N_i data in each radial bin i we compute the average weighted rotation velocity, where the weights are taken from the uncertainties in the rotation velocities (given online).

In Table 2, we report the 14 r_i positions, the values of the co-added double normalized curve $v = V(R/R_{opt})/V(R_{opt})$ and of their uncertainties dv, calculated as the standard deviation with respect to the mean.[6] The universality of this curve can be inferred from its very small rms values (see Fig. 3). Furthermore, we investigate the universality in deep by calculating the residuals of each individual RC with respect to the emerging co-added curve (Table 2 column 5):

$$\chi^2 = \frac{\sum_{ij} \frac{(v_{ij}-v_i)^2}{\delta_{ij}^2}}{N}, \quad (1)$$

where v_{ij} are the individual RC data referring to the bin i of the double normalized RC of the j dds (j from 1 to 36), v_i is the double normalized co-added i value (i from 1 to 14) [see Fig. 3], δ_{ij} are the observational errors of the normalized circular velocities and N is the total number of the data points ($N = 350$).[7]

We consider the 14 v_i as an exact numerical function that we attempt to fit with double normalized velocity data v_{ij}: we found that the fit is excellent, the reduced chi-square is ∼1.0 and the reduced residuals $dv_{ij} = v_{ij} - v_i$ are very small, see Fig. 4. In fact ∼72 per cent of the residuals is smaller than 1 δ_{ij}, ∼26 per cent falls inside 3 δ_{ij} and only the remaining ∼2 per cent is anomalously large.

[6] Lowercase letters refer to normalized values, while capital letters to the values in physical units.

[7] i is the index number of a radial bin and ij are the index numbers of a data j in a bin i.

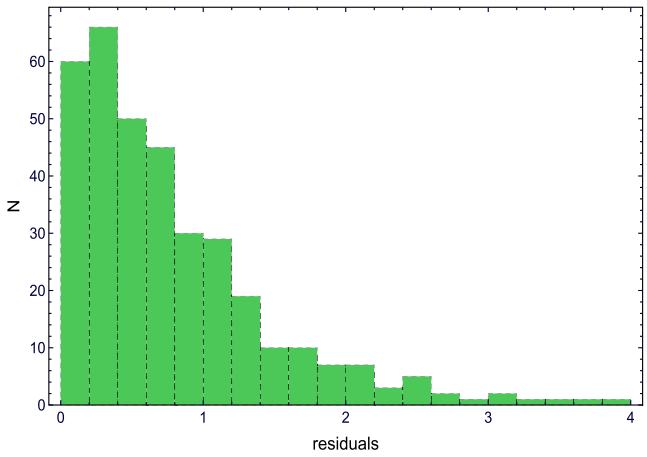

Figure 4. The distribution of residuals in terms of rms, which are listed in column 5 of Table 2.

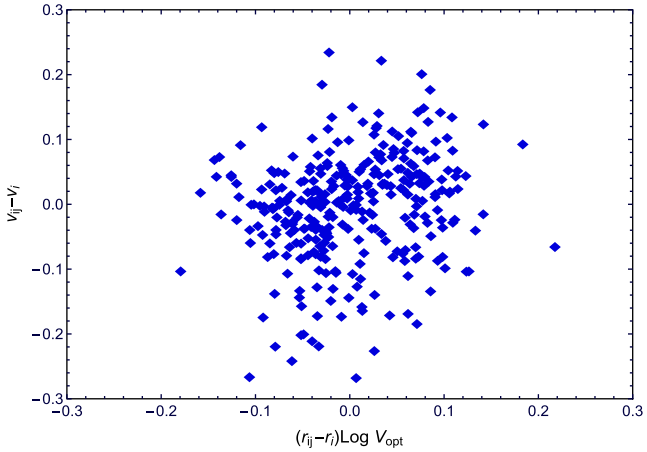

Figure 5. The v_{ij} residuals in the 14 bins versus the optical velocity log V_{opt}. Coefficient of correlation R^2 is ∼0.06.

Finally, in order to check the existence of biases, we investigate, in all 14 bins, whether the dv_{ij} residuals have any correlation with the optical velocity log V^{ij}_{opt} of the corresponding galaxy (see Fig. 5). However, we did not find any correlation, see Fig. 5; dd galaxies of any luminosity (and V_{opt}) show the same double normalized RC profile. Indeed, our accurate analysis shows no evidence of dd with a double normalized RC to be different from the co-added $v_i(r_i)$ derived in this section and given in Table 2.

Hereafter, it is worth comparing the present results with those of PSS; in the left-hand panel of Fig. B1, the former is plotted alongside with the similar curves of the four PSS luminosity bins (see also fig. 6 in PSS). The least luminous bin of PSS (red joint circles in Fig. B1) contains 40 normal spirals with the average I-band magnitude of $\langle M_I \rangle = -18.5$. Noticeably, the two double normalized co-added RCs are in good agreement, keeping in mind that, in this work, the luminosity bin $-19 \lesssim M_I \lesssim -13$ is as big as the whole luminosity range of PSS that, instead, was divided in 11 bins.

Thus, starting from $M_I \sim -18.5$ and down to the faintest systems, the mass structure of disc galaxies is just a dark halo with a density core radius as big as the stellar disc. At $M_I \gtrsim -18.5$, the stellar disc contribution disappears and, remarkably, the RC profile becomes solid body like $V(R) \propto R$.

We now investigate quantitatively the last statement: one can notice that the co-added RC of dds is slightly shallower than that of the least luminous spirals of PSS (see left-hand panel of Fig. B1 and Appendix B). Therefore, we check for the presence of any trend between luminosity and shape of the corresponding RC inside our sample of 36 dds. We divide them in three subsamples (12 galaxies each, ordered by their luminosity). Then, we derive the three corresponding stacked RCs (see Table B1). No trend between RC shape and luminosity was found, differently from what it occurs for spirals of higher luminosity, see Appendix B and Fig. B1.

Finally, let us point out that neither the double normalization nor the stacking of our 36 objects is the cause of the solid body profile of the RC in Fig. 3 and Table 2. The reason is that each RC of our sample, also when considered in physical units, shows, inside $2R_D$, a solid body profile.

Therefore, we conclude the existence of the co-added RC for the dd population. This is the first step to obtain that the kinematics of dd galaxies can be described by a smooth universal function, exactly as it happens in normal spirals (PSS, Salucci et al. 2007).

4 MODELLING THE DOUBLE NORMALIZED CO-ADDED RC OF DWARF DISC GALAXIES

As in normal spirals (see PSS), we mass model the co-added RC data that represent the whole kinematics of dds. More precisely,

1. the co-added (double normalized) RC (see Table 2), once proven to be universal, is the basic data with which we build the mass model of dd galaxies;

2. for simplicity, we rescale the 14 normalized velocities v_i to the average values of the sample $\langle V_{opt} \rangle$ and $\langle R_{opt} \rangle$, 40.0 km s^{-1} and 2.5 kpc, respectively. In details, we write

$$\langle V_i \rangle = v_i \langle V_{opt} \rangle;$$
$$\langle R_i \rangle = r_i \langle R_{opt} \rangle, \quad (2)$$

the 14 values of $\langle V_i \rangle$ and $\langle R_i \rangle$ are also reported in Table 2 (columns 6–7), where angle brackets indicate normalization to the average values of optical radius and to the log average values of optical velocity. This RC is the fiducial curve for dd systems. In fact, we take the co-added curve in Table 2 (columns 3–5) and we apply it to a galaxy with the values of R_{opt} and V_{opt} equal to the average values in our sample. Since all dd RCs have the same double normalized profile, the parameters of the resulting mass model can be easily rescaled back to cope with galaxies of different V_{opt} and R_{opt}.

The fiducial RC (Table 2 columns 6–8) of dds consists of 14 velocity data points extended out to 1.9 $\langle R_{opt} \rangle$. The uncertainties on the velocities are at the level of ∼3 per cent (see Fig. 3).

Then, the circular velocity model $V_{tot}(R)$ consists into the sum, in quadrature, of three terms V_D, $V_{H\,I}$, V_{DM} that describe the contribution from the stellar disc, the H I disc and dark halo, and that must equate to the observed circular velocity:

$$V^2_{tot}(R) = V_m(R) \equiv V^2_D(R) + V^2_{H\,I}(R) + V^2_{DM}(R). \quad (3)$$

Note that in the right-hand side of equation (3), we have neglected the stellar bulge contribution that is, in fact, absent in dds.

4.1 Stellar component

With a constant stellar-mass-to-light ratio as function of radius (see e.g Bell & de Jong 2001), all 36 dds have the same surface density stellar profile Σ_D well represented by the Freeman disc (Freeman 1970):

$$\Sigma_D(R) = \frac{M_D}{2\pi R^2_D} e^{-\frac{R}{R_D}} \quad (4)$$

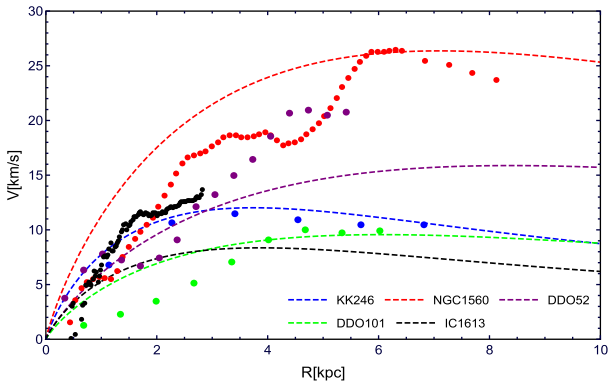

Figure 6. The observed circular velocities of H I taking from Gentile et al. (2010), Gentile et al. (2012) and Oh et al. (2015, points), and the approximation for the distribution of H I component as described in Tonini et al. (2006, dashed lines).

then, the contribution of the stellar disc $V_{\rm D}(R)$ is

$$V_{\rm D}^2(R) = \frac{1}{2}\frac{GM_{\rm D}}{R_{\rm D}}(3.2x)^2(I_0K_0 - I_1K_1), \quad (5)$$

where $x = R/R_{\rm opt}$ and I_n and K_n are the modified Bessel functions computed at $1.6x$.

4.2 Gas disc

For each galaxy, the gaseous mass $M_{\rm H\,I}$ was taken from K13, log averaged and then multiplied by a factor 1.33 to account for the He abundance, then we obtain $\langle M_{\rm H\,I}\rangle = 1.7 \times 10^8\,{\rm M}_\odot$. The H I surface density profile is not available for all dd galaxies of our sample, therefore we model it, by following Tonini et al. (2006), as a Freeman distribution with a scalelength three times larger that of the stellar disc $\Sigma_{\rm H\,I}(R) = \frac{M_{\rm H\,I}}{2\pi(3R_{\rm D})^2}{\rm e}^{-\frac{R}{3R_{\rm D}}}$. Then, the contribution of the gaseous disc $V_{\rm H\,I}(R)$ is

$$V_{\rm H\,I}^2(R) = \frac{1}{2}\frac{GM_{\rm H\,I}}{3R_{\rm D}}(1.1x)^2(I_0K_0 - I_1K_1), \quad (6)$$

where $x = R/R_{\rm opt}$ and I_n and K_n are the modified Bessel functions computed at $0.53x$.

This scheme is fairly well supported in dds for which the H I surface density data are available (e.g. data from Gentile et al. 2010, 2012; Oh et al. 2015). In order to clarify the latter, we plot in Fig. 6, alongside the observed RC of H I component and our approximation of the H I distribution for five galaxies of our sample.

In addition, let us stress that the gas contribution is always a minor component to the dds circular velocities, consequently possible errors in its estimate do not alter the mass modelling neither affect any result of this paper.

4.3 Dark halo

Many different halo radial mass profiles have been proposed over the years. Thus, in this work we are going to test the following profiles.

4.3.1 Burkert profile

The URC of normal spirals and the kinematics of individual objects (Salucci & Burkert 2000) point to dark haloes density profiles with a constant core, and, in particular, to the Burkert halo profile (Burkert 1995), for which

$$\rho_{\rm B,URC}(r) = \frac{\rho_0 r_{\rm c}^3}{(r + r_{\rm c})(r^2 + r_{\rm c}^2)}, \quad (7)$$

where ρ_0 (the central density) and $r_{\rm c}$ (the core radius) are the two free parameters and $\rho_{\rm B,URC}$ means that we have adopted the Burkert profile for the URC DM halo component. Hereafter, we will freely exchange the two denominations according to the issue considered.

Adopting spherical symmetry, the mass distribution of the Burkert haloes is given by

$$M_{\rm URC}(r) = 2\pi\rho_0 r_{\rm c}^3\left[\ln\left(1+\frac{r}{r_{\rm c}}\right) - tg^{-1}\left(\frac{r}{r_{\rm c}}\right) + 0.5\ln\left(1+\left(\frac{r}{r_{\rm c}}\right)^2\right)\right]. \quad (8)$$

4.3.2 NFW profile

We will investigate also NFW profile. Navarro et al. (1996b) found, in numerical simulations performed in the (Λ)CDM scenario of structure formation, that virialized systems follow a universal DM halo profile. This is written as

$$\rho_{\rm NFW}(r) = \frac{\rho_0}{\left(\frac{r}{r_{\rm s}}\right)\left(1+\frac{r}{r_{\rm s}}\right)^2}, \quad (9)$$

where ρ_0 and $r_{\rm s}$ are, respectively, the characteristic density and the scale radius of the distribution. These two parameters can be expressed in terms of the virial mass $M_{\rm vir} = 4/3\pi 100\rho_{\rm crit}R_{\rm vir}^3$, the concentration parameter $c = \frac{R_{\rm vir}}{r_{\rm s}}$ and the critical density of the Universe $\rho_{\rm crit} = 9.3 \times 10^{-30}{\rm g\,cm^{-3}}$. By using equation (9), we can write

$$\rho_0 = \frac{100}{3}\frac{c^3}{\log(1+c) - \frac{c}{1+c}}\rho_{\rm crit} \quad {\rm g\,cm^{-3}};$$

$$r_{\rm s} = \frac{1}{c}\left(\frac{3\times M_{\rm vir}}{4\pi 100\rho_{\rm crit}}\right)^{1/3} \quad {\rm kpc}. \quad (10)$$

Then, the RC curve for the NFW DM profile is

$$V_{\rm NFW}^2(r) = V_{\rm vir}^2\frac{\log(1+cx) - cx/(1+cx)}{x[\log(1+c) - c/(1+c)]}, \quad (11)$$

where $x = r/R_{\rm vir}$ and $V_{\rm vir}$ represents the circular velocity at $R_{\rm vir}$.

Let us point out that, within the (Λ)CDM scenario, the NWF profile maybe not the present-day dark haloes around spirals. Baryons, during the formation of the stellar discs, may have been able to modify the original DM density distributions (see, e.g. Pontzen & Governato 2012, 2014; Di Cintio et al. 2014). We then consider equation (11) as the fiducial profile of (Λ)CDM scenario, a working assumption useful to frame changes of the latter.

4.3.3 DC14 profile

A solution for the existence of cored profiles in (Λ)CDM scenario may have emerged by considering the recently developed DM density profile (see Di Cintio et al. 2014). This profile (hereinafter referred to as DC14) accounts for the effects of feedback on the DM haloes due to gas outflows generated in high-density star-forming regions during the history of the stellar disc. The resulting radial profile is far from simple, since it starts from an (α, β, γ) double power-law model (DC14)

$$\rho_{\rm DC14}(r) = \frac{\rho_{\rm s}}{\left(\frac{r}{r_{\rm s}}\right)^{\gamma}\left(1+(\frac{r}{r_{\rm s}})^{\alpha}\right)^{\frac{(\beta-\gamma)}{\alpha}}}, \quad (12)$$

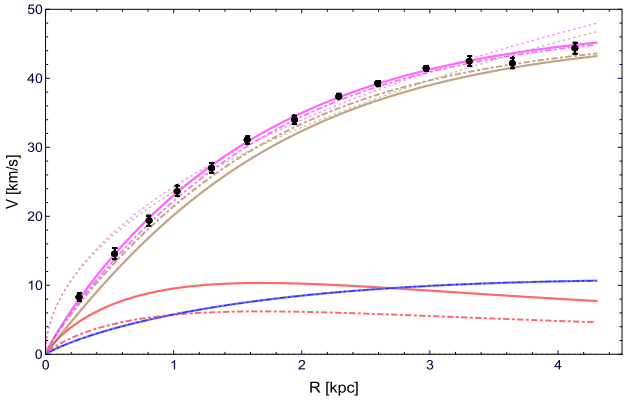

Figure 7. The synthetic RC (filled circles with uncertainties) and URC with its separate dark/luminous contributions (red line: disc; blue line: gas; brown line: halo; pink line: the sum of all components) in case of three DM profiles: the Burkert DM profile (solid lines), NFW profile (dashed lines) and DC14 profile (dot–dashed line).

where ρ_s is the scale density and r_s the scale radius. The inner and the outer regions have logarithmic slopes $-\gamma$ and $-\beta$, respectively, and α indicates the sharpness of the transition. These three parameters are fully constrained in terms of the stellar-to-halo mass ratio as shown in DC14:

$$\alpha = 2.94 - \log_{10}\left[\left(10^{X+2.33}\right)^{-1.08} + \left(10^{X+2.33}\right)^{2.29}\right]$$
$$\beta = 4.23 + 1.34X + 0.26X^2$$
$$\gamma = -0.06 + \log_{10}\left[\left(10^{X+2.56}\right)^{-0.68} + \left(10^{X+2.56}\right)\right] \quad (13)$$

where $X = \log_{10}\left(\frac{M_D}{M_{\rm halo}}\right)$.

Then, using the definition of the enclosed mass, we can write down the expression for the scale density of the DC14 profile:

$$\rho_s = M_{\rm vir}/4\pi \int_0^{R_{\rm vir}} \frac{r^2}{\left(\frac{r}{r_s}\right)^{\gamma}\left[1+\left(\frac{r}{r_s}\right)^{\alpha}\right]^{\frac{\beta-\gamma}{\alpha}}} {\rm d}r. \quad (14)$$

Finally, by combining the above equations (12)–(14), we obtain a density profile as a function of three parameters r_s, $M_{\rm halo}$ and M_D, which we use in order to define the RC curve for the DC14 DM profile.

Despite the complexity of the proposed scheme, it is worth to test such DM density profile based on the analysis of hydro-dynamically simulated galaxies (DC14) drawn from the MaGICC project (Brook et al. 2012; Stinson et al. 2013).

4.4 Results

In Fig. 7, we show the results of the mass modelling of the fiducial RC by means of the dwarf disc universal rotation curve (‘dd’URC) model: an exponential Freeman disc, a gaseous disc plus a Burkert halo profile. This result is very successful (see solid lines of Fig. 7) with $\chi^2_{\rm red} < 1$. The best-fitting parameters of the fiducial RC are

$$\log\langle\rho_0\rangle = 7.55 \pm 0.04 \quad {\rm M}_\odot\,{\rm kpc}^{-3};$$
$$\langle r_c\rangle = 2.30 \pm 0.13 \quad {\rm kpc};$$
$$\log\langle M_D\rangle = 7.71 \pm 0.15 \quad {\rm M}_\odot. \quad (15)$$

The resulting virial mass is $\langle M_{\rm vir}\rangle = (1.38 \pm 0.05) \times 10^{10}\,{\rm M}_\odot$.

It is worth to recall that the co-added double normalized RC of dds (Table 2 columns 3–5) would be identically well fitted and the relative structure parameters can easily be obtained via the transformation laws in equation (2).

NFW profile fails to reproduce the synthetic RC (see dotted lines of Fig. 7), the reduced chi-square is ≈12 and the best-fitting parameters

$$\log\langle M_{\rm vir}\rangle = 11.68 \pm 0.87 \quad {\rm M}_\odot;$$
$$\langle c\rangle = 4.73 \pm 3.19;$$
$$\log\langle M_D\rangle = 2.50^{+?}_{-2.50} \quad {\rm M}_\odot,$$

lead to totally unrealistic estimates of the stellar disc and halo masses.

The DC14 profile shows the same good-quality fit (see dot–dashed lines of Fig. 7) as the URC profile with $\chi^2_{\rm red} < 1$ and quite similar values of the structural parameters.

$$\log\langle M_{\rm vir}\rangle = 10.30 \pm 0.02 \quad {\rm M}_\odot;$$
$$\langle r_s\rangle = 2.05 \pm 0.13;$$
$$\log\langle M_D\rangle = 7.30 \pm 0.14 \quad {\rm M}_\odot.$$

Then, in spite of the fact that galaxies in our sample vary by ∼6 mag in the *I* band, we obtain a universal function of the normalized galactocentric radius, similar to that setup in PSS, that is able to fit well the double normalized co-added RCs of galaxies, when extrapolated to our much lower masses.

To summarize, we have worked out the ‘dd’URC, i.e. an analytical model for the dds co-added curve, that represents the RC of dd galaxies. This function is given by equations (3), (5) and (8) and by equation (15). Let us stress here that the ‘dd’URC can be considered as the 12th bin of the URC.

5 DENORMALIZATION OF THE ‘DD’URC MASS MODEL

In this section, we will construct a URC for the dd galaxies in the physical units that will cope with the diversity of RCs evident in Fig. 2. In spirals (see PSS), we can easily go back from a double normalized URC $V(R/R_{\rm opt})/V_{\rm opt}$ to an RC expressed in physical units $V(R/{\rm kpc}, M_I)\,{\rm km\,s^{-1}}$, where $R_{\rm opt}$, $V_{\rm opt}$ and M_I are altogether well correlated. This is not the case for dds where another quantity, the compactness, enters in the above three-quantity link.

Let us first remind that in every radial bin the residuals do not correlate with the optical velocity of the corresponding galaxy (see Section 3). This implies that the dds structural parameters of the dark and luminous matter have a negligible direct dependence on luminosity/optical velocity different from that inherent to the two normalizations we apply to the individual RCs.

Moreover, given the very small intrinsic scatter of the fiducial double normalized co-added RC and the extremely good fit of the ‘dd’URC to it, we can write

$$\frac{M_{\rm D,H\,I}}{V^2_{\rm opt}R_{\rm opt}} = \frac{\langle M_{\rm D,H\,I}\rangle}{\langle V^2_{\rm opt}\rangle\langle R_{\rm opt}\rangle} \equiv const. \quad (16)$$

Then, we derive in all objects a direct proportionality between the halo core radius r_c and the disc scalelength R_D, which is in agreement with the extrapolation of the corresponding relationship in normal spirals of much higher masses (Salucci et al. 2007): $log(r_c) = 0.47 + 1.38\log(R_D)$, see Fig. 8.

We also assume that $\frac{V^2_D(R_{\rm opt})}{V^2_{\rm H\,I}(R_{\rm opt})}$ is constant among galaxies and it equals to the value of the average case $\frac{\langle V^2_D(R_{\rm opt})\rangle}{\langle V^2_{\rm H\,I}(R_{\rm opt})\rangle} \simeq 1.1$.

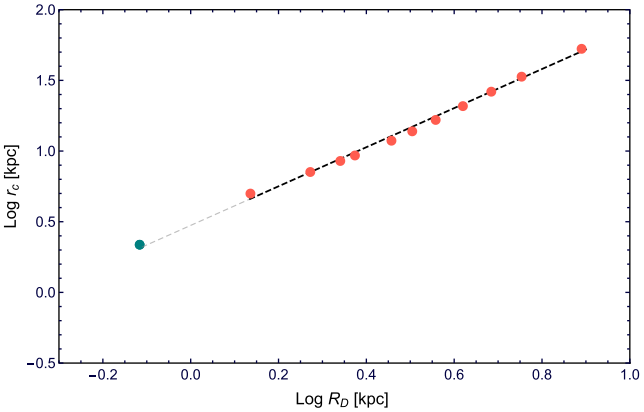

Figure 8. The core radius versus disc scalelength. Red circles represent the values of the URC of normal spirals and green circle represents the best-fitting values found in the previous section. Black dashed line is a linear fit to the data of the URC of normal spirals and the grey dashed line is the extrapolation of the linear fit to the dds regime.

Consequently with the above assumptions, for each galaxy of the sample, we have

$$M_{\rm DM}(R_{\rm opt}) = (1-\alpha)V_{\rm opt}^2 R_{\rm opt} G^{-1}, \tag{17}$$

where $M_{\rm DM}$ is the Burkert DM mass inside the optical radius $R_{\rm opt}$ and α is the fraction that baryonic matter contributes to the total circular velocity:

$$\alpha = \frac{\langle V_{\rm H\,I}^2(R_{\rm opt})\rangle + \langle V_D^2(R_{\rm opt})\rangle}{\langle V_{\rm tot}^2(R_{\rm opt})\rangle} = 0.12 \equiv const. \tag{18}$$

Note that in some galaxies the fractional contribution to V from the H I disc can be different from the assumed value of ∼0.06. However, this has no effect on our investigation. In fact, at the radii where the H I disc is more relevant than the stellar disc, the contribution of the DM halo becomes overwhelming (Evoli et al. 2011).

By simple manipulations of equations (16)–(18) inserting the individual values of $R_{\rm opt}$, $V_{\rm opt}$, we get, for each galaxy, the structural parameters of the dark and the luminous matter. In Table 3, we list them alongside with their uncertainties obtained from those of the URC mass model given in equation (15).

5.1 H I gas mass and stellar mass

We now check the validity of the assumptions in the previous subsection. We compare our estimated values of the defined galactic H I masses, equation (16), with those given by K13 (calculated using total H I flux, for more details see K13). We find

$$\log M_{\rm H\,Ikin} = (-0.015 \pm 1.12) + (1.0 \pm 0.14)\log M_{\rm H\,IK13} \tag{19}$$

with an rms of 0.3 dex. The value of the slope and the small rms, despite the presence of some outliers most probably originating from the large range in luminosities and morphologies of our sample, suggests that $M_{\rm H\,Ikin}$ are good proxies of $M_{\rm H\,IK13}$. Therefore, adopting them does not influence any result of this paper.

We also compare the kinematical derivation of the stellar disc masses for the objects in our sample with those obtained for the same objects from $K_{\rm S}$-band photometry (provided by K13). Following Bell et al. (2003) and McGaugh & Schombert (2015), we adopt a constant mass-to-light ratio of $M/L_K = 0.6 \times {\rm M}_\odot/{\rm L}_\odot$ and we report them in Table 3 as $M_{\rm D}(K_{\rm S})$. We find a good correlation between the two estimates:

$$\log M_{\rm Dkin} = (2.49 \pm 1.0) + (0.64 \pm 0.12)\log M_{{\rm D}K_{\rm S}} \tag{20}$$

with an rms of 0.4 dex. The two estimates are therefore mutually consistent especially by considering that the kinematical estimate has an uncertainty of 0.3 dex (see Salucci, Yegorova & Drory 2008). Let us also notice that in dds the conversion between luminosity and stellar masses is subject to a similarly large systematical uncertainty, especially in actively star-forming galaxies like those present in our sample.

These results, therefore, support well the scheme used in this paper to deal with the luminous components of dds.

Furthermore, we compare our results with Lelli, McGaugh & Schombert (2016), where the authors analyse a sample of 176 disc galaxies and quantify for them the ratio of baryonic-to-observed velocity. We have, that this ratio, calculated at 2.2 disc scalelengths, is ∼0.4. The latter is consistent with values of Lelli et al. (2016), established for a sample of dd galaxies. Moreover, we found that the value of gas fraction ($f_{\rm gas} \equiv \frac{M_{\rm H\,I}}{M_{\rm bar}} \sim 0.8$) in our sample is also consistent with the value estimated by Lelli et al. (2016), where the authors show that low-luminosity end disc galaxies are extremely gas dominated with $f_{\rm gas} \simeq 0.8$–1.0.

5.2 The scaling relations

Let us plot, the central surface density of the DM haloes of our sample, i.e. the product of $\rho_0 r_{\rm c}$, as a function of B magnitude (see Fig. 9). A constancy of this product has been found over 18 blue magnitudes and in objects ranging from dwarf galaxies to giant galaxies (e.g Kormendy & Freeman 2004; Donato et al. 2009; Gentile et al. 2009; Plana et al. 2010; Salucci et al. 2012; Ogiya et al. 2014). For the case of dds, in Fig. 9, one can see that most of the objects of our sample fall inside the extrapolation of Donato et al. (2009) relation (see the orange shadowed area of Fig. 9) with a scatter of about 0.3 dex of an uncertain origin.

We now work out the relationships among the various structural properties of the dark and luminous matter of each galaxy in our sample. These will provide us with crucial information on the relation between dark and baryonic matter as well as on the DM itself. Obviously these relationships are also necessary in order to establish the URC for the present sample.

We first derive the galaxy baryonic mass versus halo virial mass relation and compare it with that of normal spiral galaxies (Salucci et al. 2007), see Fig. 10. We take 0.3 dex as 1σ error in the baryonic mass (blue shadowed area). Fig. 10 highlights that galaxies of our sample, i.e. dd objects live in haloes with masses below $5 \times 10^{10}\,{\rm M}_\odot$ and above $4 \times 10^8\,{\rm M}_\odot$. A similar result was found by Ferrero et al. (2012), who analysed a sample of dd galaxies either by using the individual mass modelling or the outermost values of their RCs. In Fig. 10, we also show the comparison of our results with the relation derived from the abundance matching method by Papastergis et al. (2012). Remarkably, for $M_{\rm vir} \lesssim 4 \times 10^{10}\,{\rm M}_\odot$, it is inconsistent with the relation found from the abundance matching method and its extrapolation (see Fig. 10). Likewise, $M_{\rm bar}$–$M_{\rm vir}$ relation found for dds is significantly shallower than that of the low-mass spirals. The origin of this discrepancy is unclear. One possibility might be that we are facing a selection effect. This means that galaxies in our sample have, on average, more gas than that of

Table 3. Sample of dd galaxies. Columns: (1) galaxy name; (2) the stellar disc mass; (3) the stellar disc mass using K-band luminosities; (4) the gas mass; (5) the gas mass listed in Karachentsev et al. (2013); (6) the core radius; (7) the central density; (8) the halo mass; (9) compactness of the stellar disc.

Name	M_D	$M_D(K_S)$	$M_{H\,I}$	$M_{H\,I}$(K13)	r_c	$\log(\rho_0)$	M_h	C
–	$\times 10^7$	$\times 10^7$	$\times 10^7$	$\times 10^7$	–	–	$\times 10^9$	–
–	($M_\odot$)	($M_\odot$)	($M_\odot$)	($M_\odot$)	(kpc)	(g cm^{-3})	($M_\odot$)	–
(1)	(2)	(3)	(4)	(5)	(6)	(7)	(8)	(9)
UGC1281	9.8	19.9	38.7	22.1	2.93	−23.6	32.4	1.1
UGC1501	11.3	23.9	44.3	38.4	4.32	−23.9	40.2	0.88
UGC5427	3.74	8.28	14.7	3.93	0.76	−22.5	8.89	1.86
UGC7559	4.19	7.21	16.5	13.9	2.46	−23.8	11.9	0.84
UGC8837	12.0	24.4	47.2	29.8	5.40	−24.1	44.6	0.77
UGC7047	2.65	11.4	10.4	15.3	1.34	−23.3	6.53	1.05
UGC5272	13.2	6.58	53.0	23.1	4.14	−23.8	48.1	0.98
DDO52	16.0	14.7	62.9	27.8	4.24	−23.8	60.1	1.05
DDO101	11.1	49.9	43.7	16.0	2.71	−23.4	36.8	1.22
DDO154	3.70	2.33	14.6	25.3	1.98	−23.6	10.0	0.93
DDO168	10.2	8.28	40.2	29.8	2.28	−23.3	32.5	1.33
Haro29	1.02	3.96	4.02	7.65	0.51	−22.6	2.02	1.37
Haro36	10.6	13.8	41.7	14.9	2.84	−23.5	35.1	1.16
IC10	2.19	17.7	8.61	13.3	0.78	−22.8	4.94	1.43
NGC2366	13.3	28.1	52.1	54.2	4.16	−23.8	48.2	0.97
WLM	2.05	2.94	8.05	9.0	1.29	−23.4	4.86	0.96
UGC7603	13.8	53.5	54.4	55.4	3.42	−23.6	49.0	1.14
UGC7861	7.87	97.3	30.9	41.1	1.51	−23.0	22.6	1.59
NGC1560	11.8	31.5	46.5	142.5	3.37	−23.7	40.9	1.08
DDO125	0.49	7.55	1.91	4.02	1.1	−23.8	0.93	0.56
UGC5423	2.77	15.4	10.9	9.2	1.19	−23.14	6.76	1.17
UGC7866	1.53	9.29	6.02	10.6	1.27	−23.5	3.49	0.85
DDO43	2.42	2.44	9.72	9.42	1.35	−23.3	5.92	1.0
IC1613	0.74	7.05	2.91	7.8	1.46	−23.9	1.53	0.55
UGC4483	0.28	0.6	1.09	4.4	0.29	−22.6	4.513	1.12
KK246	2.38	3.96	9.35	15.6	1.40	−23.4	5.82	0.98
NGC6822	2.34	13.1	9.21	18.8	1.32	−23.3	5.68	1.01
UGC7916	7.63	3.79	30.0	35.8	5.80	−24.4	26.3	0.59
UGC5918	8.43	12.3	33.2	23.1	3.88	−23.9	28.3	0.83
AndIV	1.68	0.77	6.62	27.8	1.06	−23.2	3.81	1.02
UGC7232	0.99	3.91	4.0	3.84	0.34	−22.2	1.88	1.77
DDO133	5.53	10.4	21.7	21.1	2.55	−23.7	16.4	0.93
UGC8508	0.62	2.43	2.48	2.65	0.50	−22.8	1.15	1.10
UGC2455	8.03	122.5	31.5	87.9	3.21	−23.8	26.0	0.93
NGC3741	0.33	1.44	1.31	10.1	0.27	−22.4	0.55	1.31
UGC11583	10.9	5.73	42.9	24.8	3.67	−23.8	37.8	0.97

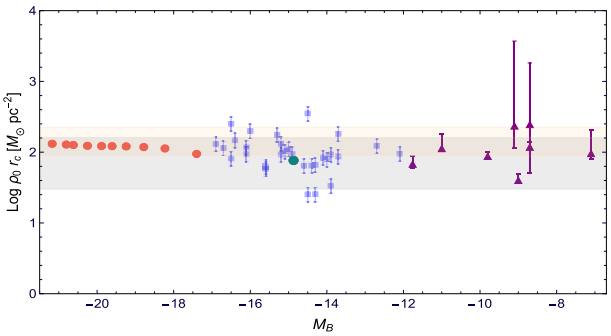

Figure 9. $\rho_0 r_c$ in units of $M_\odot$ pc^{-2} as a function of a galaxy magnitude for different galaxies and Hubble types. The data are: the Salucci et al. (2012) URC of normal spiral galaxies (red circles); scaling relation from Donato et al. (2009, orange shadowed area); Milky Way dSphs (purple triangles) Salucci et al. (2012); dd galaxies (blue squares – this work, green dot represents the average point), B magnitudes are taking from KK13; empirically inferred scaling relation: $\rho_0 r_c = 75^{+85}_{-45}\,M_\odot$ pc^{-2} from Burkert (2015, grey shadowed area).

the Papastergis et al. (2012) sample. We check it by excluding the gaseous mass and then comparing the stellar disc mass versus the virial mass relation of our sample with that derived from the abundance matching method (we use the relation of Moster et al. 2013), see Fig. 11. Remarkably, although there is still discrepancy between the M_D–M_{vir} relation of the URC and that of the Moster et al. (2013), however it shifted to the lower masses. Furthermore, let us stress that the fit resulting from the baryon-influenced DC14 profile has a lower value of the disc mass. Consequently, the derived baryonic mass against the virial mass value for the DC14 profile comes quite close to the extrapolation of the abundance matching relation of Papastergis et al. (2012), see Fig. 10. Along with that, the derived stellar disc mass against the virial mass value for the DC14 profile agrees, within the errors, with the extrapolation of the abundance matching relation of Moster et al. (2013), see Fig. 11. However, to investigate properly this issue we should derive the transformations laws for the DC14 profile similar to that of the Burkert profile described in Section 5. The latter is beyond the scope of this paper and we are going to address this in future work.

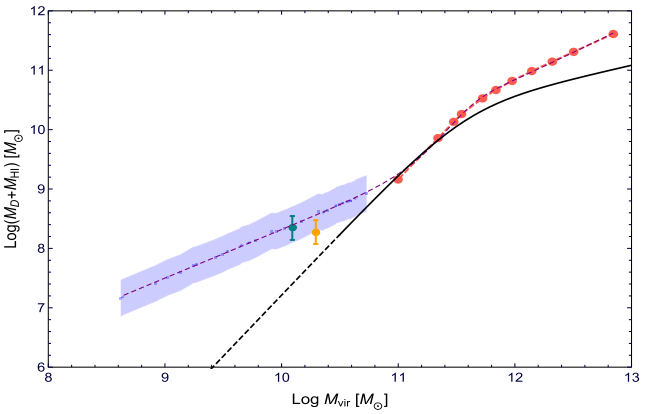

Figure 10. The baryonic mass versus the virial mass for normal spirals (joined red circles) and for the dds assuming the URC model (blue shadowed area assuming 0.3 dex scatter, the green circle with error bars represents the average point of the region). Yellow dot with error bars is the best-fitting value for the fiducial RC using DC14 model (see Section 4). Purple dashed line corresponds to the parametrized equation (21) of the galaxy baryonic mass as a function of halo mass. The abundance matching relation from Papastergis et al. (2012) is shown by black solid line, the region that is extrapolated from the Papastergis et al. (2012) relation is dashed.

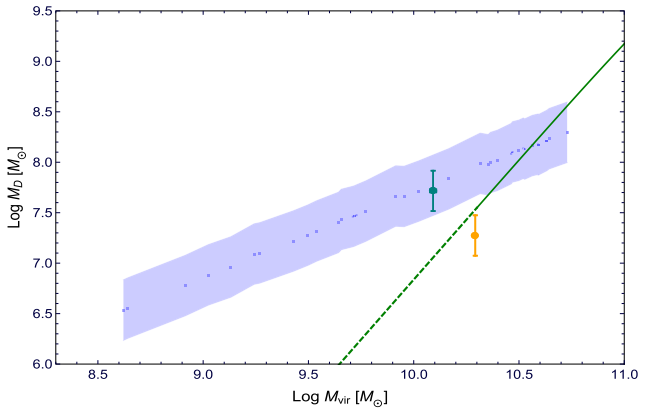

Figure 11. The disc mass versus the virial mass. Blue shadowed area represents the relation for the dds assuming the URC model and taking into account 0.3 dex scatter, the green circle with error bars represents the average point of the region. Yellow dot with error bars corresponds to the best-fitting value for the fiducial RC using DC14 model (see Section 4). The stellar mass-to-halo mass relation from Moster, Naab & White (2013) is shown by green solid line, the region that is extrapolated from the Moster et al. (2013) relation is dashed.

Note that there is also some discrepancy (irrelevant to the results of this paper) in the baryonic to halo mass relation also at higher masses. The latter is most likely due to the difference of Hubble types in the samples and in the analysis used to obtain these relations.

Then, we derive our galaxy baryonic mass versus halo virial mass relation by fitting it with the function of seven free parameters advocated by Ferrero et al. (2012) :

$$M_{\rm bar} = M_{\rm vir} \times A \left(1 + \left(\frac{M_{\rm vir}}{10^{M_1}}\right)^{-2}\right)^{\kappa} \times \left(\left(\frac{M_{\rm vir}}{10^{M_0}}\right)^{-\alpha} + \left(\frac{M_{\rm vir}}{10^{M_0}}\right)^{\beta}\right)^{-\gamma}, \quad (21)$$

we found $A = 0.070$, $\kappa = 1.85$, $M_1 = 11.34$, $M_0 = 11.58$, $\alpha = 3.34$, $\beta = 0.043$ and $\gamma = 1.05$ (purple dashed line of Fig. 10).

The other two relationships which are necessary to establish the URC of dds also in physical units i.e. $R_{\rm D}$–$M_{\rm vir}$ or ρ_0–$r_{\rm c}$, show a very large scatter (see Fig. 12) as a consequence of the presence of dd galaxies in the sample (and in the Universe) with almost the same stellar mass (luminosity) but with a different size of their stellar discs. At face value, relationships in Fig. 12 may lead us to exclude the existence of the URC in physical units for dd galaxies. In fact, the large scatter in Fig. 12 requires a new parameter to restore it.

Therefore, we proceed and show that the universality is restored by introducing a new parameter, which we call 'compactness' C. We define, for galaxies in the (dd) sample, the quantity C as the ratio between the value predicted from the measured galaxy disc mass $M_{\rm D}$ according to the simple linear regression $R_{\rm D}$ versus $M_{\rm D}$ of the whole sample and that of $R_{\rm D}$ measured from photometry. As regard, we find

$$\log R_{\rm D} = -3.64 + 0.46 \log M_{\rm D}. \quad (22)$$

Then, we obtain the following expression of C,

$$C = \frac{10^{(-3.64+0.46\ \log\ M_{\rm D})}}{R_{\rm D}} \quad (23)$$

that obviously describes the differences of the sizes of the stellar discs reduced at a same stellar mass. C varies from 0.96 to 1.02 and its distribution in our sample is listed in Table 3.

By fitting $\log R_{\rm D}$ to $\log M_{\rm vir}$ with an additional variable $\log C$, we obtain an excellent fit shown in Fig. 13. The model function being,

$$\log R_{\rm D} = -3.99 + 0.38 \log M_{\rm vir} - 0.94 \log C. \quad (24)$$

This relation just acknowledges the existence of another player in the stellar disc mass-size interplay.

Then, we fit $\log\rho_0$ to $\log M_{\rm vir}$ and $\log C$:

$$\log\rho_0 = -18.26 - 0.51 \log M_{\rm vir} + 3.44 \log C. \quad (25)$$

Finally, we fit $\log \rho_0$−$\log r_{\rm c}$ by adding $\log C$ as a free parameter. The result of the fit is shown on Fig. 14 and the model function is,

$$\log\rho_0 = -23.14 - 0.97 \log r_{\rm c} + 2.18 \log C. \quad (26)$$

It is remarkable that a basic property of the stellar discs enters to set the relationship between two DM structural quantities. Therefore, the scatter, which appears in dds when we try to relate the local properties of either baryonic or DM can be eliminated by using an additional parameter C. Let us note here, that very few galaxies of the PSS least luminous bin have structural properties that overlap with those of the galaxies in our sample (see, e.g. Fig. 2). In future work, we will investigate the exact details of the onset of the C compactness regime. This is clearly necessary for constructing the URC and, on the theoretical side, the need of an additional parameter in the mass model of the late-type galaxies has to have important implications. At the same time, it will be also interesting to investigate whether, in normal spirals of PSS sample, the C compactness plays any role in defining the URC. Note, however, that we already know, in view of the small scatter of the Radial Tully relation (Yegorova & Salucci 2007), that the spirals RCs have a small dependence from another parameter beyond the luminosity/mass.

Then, analogously to the compactness of the stellar disc, we define $C_{\rm DM}$ as the compactness of the DM halo. This quantity is the ratio, galaxy by galaxy, between the DM core radius $r_{\rm c}$ (see column 6 of Table 3) and the predicted value that we obtain from the simple linear regression between $r_{\rm c}$ and $M_{\rm vir}$, which reads

$$\log r_{\rm c} = -5.08 + 0.53 \log M_{\rm vir}. \quad (27)$$

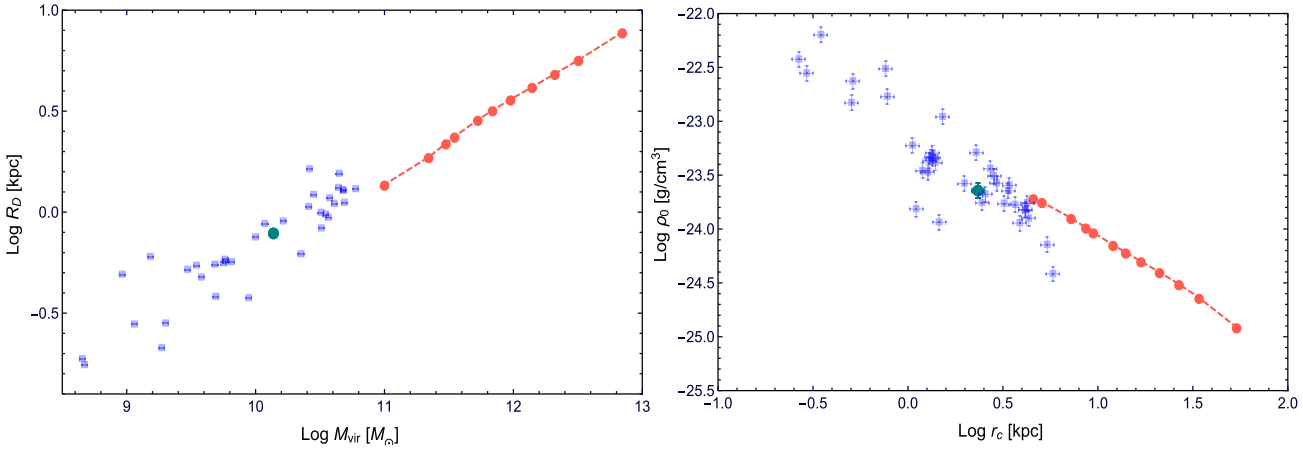

Figure 12. Left-hand panel: the disc scalelength versus virial mass. Right-hand panel: the central density versus core radius. Red circles represent normal spirals, blue squares with error bars correspond to dds of this work and the green circle with error bars represents the average point.

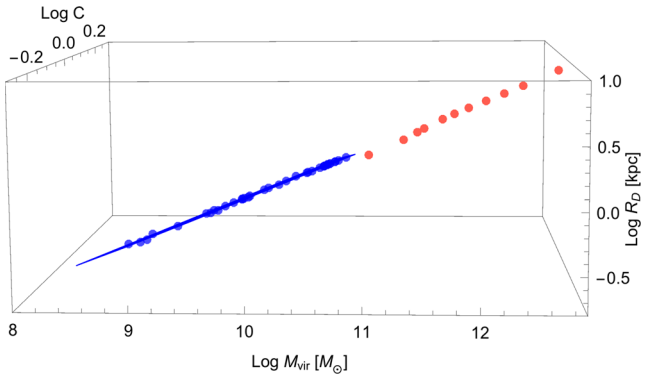

Figure 13. The disc scalelength versus virial mass and the compactness parameter C. Red circles represent normal spirals, blue squares with error bars correspond to dds of this work and blue line is the result of the fit (for details see text).

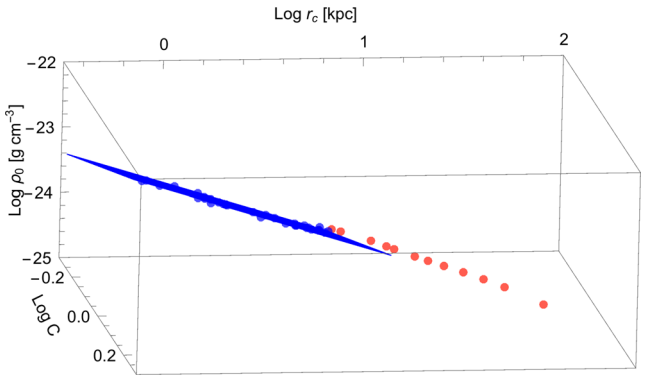

Figure 14. The central density versus core radius and the compactness parameter C. The lines and symbols are as in Fig. 13.

Then, we have

$$C_{\rm DM} = \frac{10^{-5.08+0.53\log M_{\rm vir}}}{r_{\rm c}}. \quad (28)$$

We find that the compactness of the stellar disc is closely related to the compactness of the DM halo, see Fig. 15. Consequently, the DM and the stars distributions follow each other very closely. This is extremely remarkable: it may indicate a non-standard nature of the DM or the fact that baryonic feedbacks easy the cusp core problem in a Weakly interacting massive particles scenario (see, e.g. Teyssier et al. 2013; Di Cintio et al. 2016; Dutton et al. 2016; El-Badry et al. 2016).

Finally, by using equations (5), (6), (8), (21), (23)–(26) we derive $V_{\rm `dd'URC}(R, M_{\rm D}, R_{\rm D}, C)$ the universal function that describes the dd RCs in physical units. Differently, from galaxies of higher masses it has three parameters, disc mass $M_{\rm D}$, disc scalelength $R_{\rm D}$ and concentration C, to account for the diversity of the mass distribution of these galaxies.

6 SUMMARY AND CONCLUSIONS

We have compiled literature data for a sample of dd galaxies in the local volume ($\lesssim$11 Mpc) with H I and Hα RCs. Then for these galaxies we establish the corresponding URC in normalized and physical units and investigate the related dark and luminous matter properties, not yet studied statistically in these objects. Our sample spans $\sim$2 decades ($\sim 10^6$–3×10^8 L$_\odot$) in luminosity, which coincides with the faint end of the luminosity function of disc galaxies. In magnitude, extension is as large as the whole range of normal spirals usually investigated in terms of URC. For example, the galaxies in the sample are up to $\sim$4 mag fainter than the lowest limit in the PSS sample.

We find that the large variations of our sample in luminosity and morphologies require double normalization. Notably, after this normalization we have that all RCs in double normalized units are alike. This implies that the structural parameters of the dark and luminous matter of these galaxies do not have any explicit dependence on luminosity except those coming from the normalizing process. Additionally, the good agreement of our co-added RC with that of the first PSS luminosity bin indicates that in such small galaxies the mass structure is already dominated by a dark halo with a density core as big as a stellar disc.

Then by applying to the double normalized RC the standard χ^2 mass modelling, we tested three DM density profiles. Wherein the NFW profile fails to reproduce the co-added curve, while the Burkert and DC14 profiles show excellent quality fits with $\chi^2_{\rm red} < 1$. This result points towards the cored DM distribution in dd galaxies. The same conclusion was drawn in the papers on Things and Little Things samples (see, e.g. Oh et al. 2011, 2015), where the authors found for their dwarfs much shallower inner logarithmic DM density slopes than those predicted by DM-only (Λ)CDM simulations. The present analysis has the advantages of bigger statistics, but above

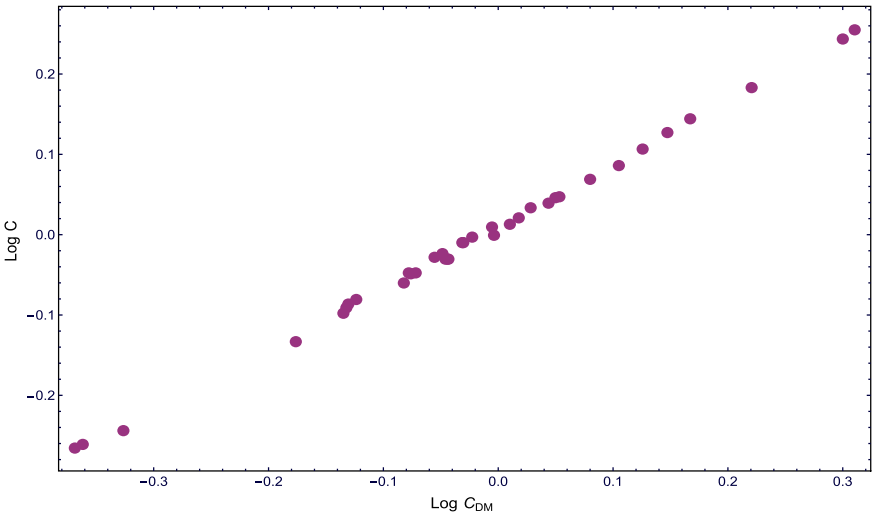

Figure 15. The compactness of the stellar disc versus the compactness of the DM halo.

all, is immune from systematics that can affect the mass modelling of individual galaxies.

We also defined, galaxy by galaxy, the values of the dark and luminous matter structural parameters. Surprisingly, a new actor enters the scene of the distribution of matter in galaxies, the compactness of the stellar component, which allows us to establish the URC in these low-mass galaxies. However, in order to understand better the role of this compactness it is required to investigate galaxies in the transition regime which appears at about $V(R_{\rm opt}) \simeq 60\,{\rm km\,s^{-1}}$.

As a consequence of the derived mass distributions, there is no evidence for the sharp decline in the baryonic to halo mass relation. Similar result, for dwarf galaxies in the field, was found by Ferrero et al. (2012). Nevertheless, notice that in DC14 case the estimated baryonic mass is slightly lower than that of the URC mass model, which brings it closer to the abundance matching relation inferred from e.g. Papastergis et al. (2012). Furthermore, since the fit resulting from the baryon-influenced DC14 profile has a lower value of the disc mass, it agrees, within the errors, with the extrapolation of the $M_{\rm D}$–$M_{\rm vir}$ relation derived from the abundance matching by Moster et al. (2013). Let us also recall that the DC14 model has been already tested against observations in works by Katz et al. (2016) and Pace (2016). Although both groups use similar methods, the drawn conclusions are different (see also Read et al. 2016). Therefore, the consistency level between observations and the (Λ)CDM model of galaxy formation, specifically the abundance matching technique deserves further investigation.

At the same time, the S-shape of $M_{\rm vir}$–$M_{\rm bar}$ relation may be interpreted as different physical mechanism occurring along the mass sequence of disc galaxies. Theoretically, it has been shown that the energetics of star formation differ among different galaxies with a characteristic dependence on the halo-to-stellar mass ratio (DC14; Chan et al. 2015) and possibly also on star formation history (Oñorbe et al. 2015).

We remark that we found that the DM and the stellar distribution follow each other very closely out to the level for which, in log–log frame, the compactness of the stellar disc is proportional to that of the DM halo. We believe that here we are touching a crucial aspect in the DM issue, whose investigation, however, much exceed the scope of this paper.

Finally, we would like to stress that the results of this work (and of the previous works, see, e.g. Donato et al. 2009; Gentile et al. 2009) indicate that the DM around galaxies should be considered, rather than the final product of the cosmological evolution of the massive components of the Universe, galaxies, today, but as the direct manifestation of one of its most extraordinary mysteries.

ACKNOWLEDGEMENTS

We thank Gianfranco Gentile, Federico Lelli, Alexei Moiseev, Se-Heon Oh and Rob Swaters for providing their data in electronic form. We would like to acknowledge Luigi Danese, Andrea Lapi and Nicola Turini for valuable discussions. We are grateful to the anonymous referees for useful comments and suggestions. We thank Brigitte Greinöcker for language corrections. EK acknowledges the hospitality of ICTP–SAIFR through the FAPESP process 2011/11973-4, for the final stages of this work.

REFERENCES

Begum A., Chengalur J. N., 2004, A&A, 424, 509
Bell E. F., de Jong R. S., 2001, ApJ, 550, 212
Bell E. F., McIntosh D. H., Katz N., Weinberg M. D., 2003, ApJS, 149, 289
Binggeli B., 1994, in Meylan G., Prugniel P., eds, European Southern Observatory Conf. Dwarf Galaxies, ESO Conference and Workshop Proc. Vol. 49, p. 13
Bosma A., 2004, in Ryder S., Pisano D., Walker M., Freeman K., eds, Proc. IAU Symp. 220, Dark Matter in Galaxies. Astron. Soc. Pac., San Francisco, p. 39
Boylan-Kolchin M., Bullock J. S., Kaplinghat M., 2012, MNRAS, 422, 1203
Brook C. B. et al., 2012, MNRAS, 426, 690
Burkert A., 1995, ApJ, 447, L25
Burkert A., 2015, ApJ, 808, 158
Chan T. K., Kereš D., Oñorbe J., Hopkins P. F., Muratov A. L., Faucher-Giguère C.-A., Quataert E., 2015, MNRAS, 454, 2981
de Blok W. J. G., Bosma A., 2002, A&A, 385, 816
de Vega H. J., Sanchez N. G., 2013, preprint (arXiv:1304.0759)
de Vega H. J., Moreno O., Moya de Guerra E., Ramón Medrano M., Sánchez N. G., 2013, Nucl. Phys. B, 866, 177
de Vega H. J., Salucci P., Sanchez N. G., 2014, MNRAS, 442, 2717
Dalcanton J. J., Stilp A. M., 2010, ApJ, 721, 547
Del Popolo A., Kroupa P., 2009, A&A, 502, 733
Di Cintio A., Brook C. B., Macciò A. V., Stinson G. S., Knebe A., Dutton A. A., Wadsley J., 2014, MNRAS, 437, 415
Di Cintio A., Brook C. B., Dutton A. A., Macciò A. V., Obreja A. C., Dekel A., 2016, MNRAS, 466, L1

Donato F. et al., 2009, MNRAS, 397, 1169
Dutton A. A. et al., 2016, MNRAS, 461, 2658
El-Badry K., Wetzel A., Geha M., Hopkins P. F., Kereš D., Chan T. K., Faucher-Giguère C.-A., 2016, ApJ, 820, 131
Elbert O. D., Bullock J. S., Garrison-Kimmel S., Rocha M., Oñorbe J., Peter A. H. G., 2015, MNRAS, 453, 29
Epinat B. et al., 2008, MNRAS, 388, 500
Erroz-Ferrer S. et al., 2016, MNRAS, 458, 1199
Evoli C., Salucci P., Lapi A., Danese L., 2011, ApJ, 743, 45
Ferrero I., Abadi M. G., Navarro J. F., Sales L. V., Gurovich S., 2012, MNRAS, 425, 2817
Freeman K. C., 1970, ApJ, 160, 811
Fukugita M., Shimasaku K., Ichikawa T., 1995, PASP, 107, 945
Garrison-Kimmel S., Boylan-Kolchin M., Bullock J. S., Kirby E. N., 2014, MNRAS, 444, 222
Gentile G., Salucci P., Klein U., Vergani D., Kalberla P., 2004, MNRAS, 351, 903
Gentile G., Burkert A., Salucci P., Klein U., Walter F., 2005, ApJ, 634, L145
Gentile G., Salucci P., Klein U., Granato G. L., 2007, MNRAS, 375, 199
Gentile G., Famaey B., Zhao H., Salucci P., 2009, Nature, 461, 627
Gentile G., Baes M., Famaey B., van Acoleyen K., 2010, MNRAS, 406, 2493
Gentile G., Angus G. W., Famaey B., Oh S.-H., de Blok W. J. G., 2012, A&A, 543, A47
Gilmore G., Wilkinson M., Kleyna J., Koch A., Evans W., Wyse R. F. G., Grebel E. K., 2007, Nucl. Phys. B, 173, 15
Herrmann K. A., Hunter D. A., Elmegreen B. G., 2013, AJ, 146, 104
Hunter D. A., Elmegreen B. G., 2004, AJ, 128, 2170
Hunter D. A., Elmegreen B. G., Oh S.-H., Anderson E., Nordgren T. E., Massey P., Wilsey N., Riabokin M., 2011, AJ, 142, 121
Hunter D. A. et al., 2012, AJ, 144, 134
Jarrett T. H., Chester T., Cutri R., Schneider S. E., Huchra J. P., 2003, AJ, 125, 525
Jungman G., Kamionkowski M., Griest K., 1996, Phys. Rep., 267, 195
Karachentsev I. D., Makarov D. I., Kaisina E. I., 2013, AJ, 145, 101 (K13)
Karachentsev I. D., Chengalur J. N., Tully R. B., Makarova L. N., Sharina M. E., Begum A., Rizzi L., 2016, Astron. Nachr., 337, 306
Katz H., Lelli F., McGaugh S. S., Di Cintio A., Brook C. B., Schombert J. M., 2016, MNRAS, preprint (arXiv:1605.05971)
Klypin A., Kravtsov A. V., Valenzuela O., Prada F., 1999, ApJ, 522, 82
Klypin A., Karachentsev I., Makarov D., Nasonova O., 2015, MNRAS, 454, 1798
Kolb E. W., Turner M. S., 1990, Frontiers in Physics Vol. 69. Addison-Wesley, Redwood City, CA
Kormendy J., 1985, ApJ, 295, 73
Kormendy J., Freeman K. C., 2004, in Ryder S., Pisano D., Walker M., Freeman K., eds, Proc. IAU Symp. 220, Dark Matter in Galaxies. Astron. Soc. Pac., San Francisco, p. 377
Lelli F., Verheijen M., Fraternali F., Sancisi R., 2012, A&A, 544, A145
Lelli F., Verheijen M., Fraternali F., 2014, A&A, 566, A71
Lelli F., McGaugh S. S., Schombert J. M., 2016, ApJ, 152, 157
Lovell M. R., Frenk C. S., Eke V. R., Jenkins A., Gao L., Theuns T., 2014, MNRAS, 439, 300
McGaugh S., 2014, Galaxies, 2, 601
McGaugh S. S., Schombert J. M., 2015, ApJ, 802, 18
Martin M. C., 1998, A&AS, 131, 73
Mashchenko S., Couchman H. M. P., Wadsley J., 2006, Nature, 442, 539
Moiseev A. V., 2014, Astrophys. Bull., 69, 1
Moore B., Ghigna S., Governato F., Lake G., Quinn T., Stadel J., Tozzi P., 1999, ApJ, 524, L19
Moster B. P., Naab T., White S. D. M., 2013, MNRAS, 428, 3121
Navarro J. F., Eke V. R., Frenk C. S., 1996a, MNRAS, 283, L72
Navarro J. F., Frenk C. S., White S. D. M., 1996b, ApJ, 462, 563
Noordermeer E., van der Hulst J. M., Sancisi R., Swaters R. S., van Albada T. S., 2007, MNRAS, 376, 1513
Ogiya G., Mori M., Ishiyama T., Burkert A., 2014, MNRAS, 440, L71
Oh S.-H., de Blok W. J. G., Brinks E., Walter F., Kennicutt R. C., Jr, 2011, AJ, 141, 193
Oh S.-H. et al., 2015, AJ, 149, 180
Oman K. A. et al., 2015, MNRAS, 452, 3650
Oñorbe J., Boylan-Kolchin M., Bullock J. S., Hopkins P. F., Kereš D., Faucher-Giguère C.-A., Quataert E., Murray N., 2015, MNRAS, 454, 2092
Pace A. B., 2016, MNRAS, preprint (arXiv:1605.05326)
Papastergis E., Martin A. M., Giovanelli R., Haynes M. P., 2011, ApJ, 739, 38
Papastergis E., Cattaneo A., Huang S., Giovanelli R., Haynes M. P., 2012, ApJ, 759, 138
Papastergis E., Giovanelli R., Haynes M. P., Shankar F., 2015, A&A, 574, A113
Parodi B. R., Barazza F. D., Binggeli B., 2002, A&A, 388, 29
Persic M., Salucci P., 1991, ApJ, 368, 60
Persic M., Salucci P., Stel F., 1996, MNRAS, 281, 27
Plana H., Amram P., Mendes de Oliveira C., Balkowski C., 2010, AJ, 139, 1
Pontzen A., Governato F., 2012, MNRAS, 421, 3464
Pontzen A., Governato F., 2014, Nature, 506, 171
Read J. I., Gilmore G., 2005, MNRAS, 356, 107
Read J. I., Iorio G., Agertz O., Fraternali F., 2016, MNRAS, 462, 3628
Rubin V. C., Burstein D., Ford W. K., Jr, Thonnard N., 1985, ApJ, 289, 81
Salucci P., 2001, MNRAS, 320, L1
Salucci P., Burkert A., 2000, ApJ, 537, L9
Salucci P., Persic M., 1997, in Persic M., Salucci P., eds, ASP Conf. Ser. Vol. 117, Dark and Visible Matter in Galaxies and Cosmological Implications. Astron. Soc. Pac., San Francisco, p. 1
Salucci P., Lapi A., Tonini C., Gentile G., Yegorova I., Klein U., 2007, MNRAS, 378, 41
Salucci P., Yegorova I. A., Drory N., 2008, MNRAS, 388, 159
Salucci P., Wilkinson M. I., Walker M. G., Gilmore G. F., Grebel E. K., Koch A., Frigerio Martins C., Wyse R. F. G., 2012, MNRAS, 420, 2034
Sharina M. E. et al., 2008, MNRAS, 384, 1544
Simard L., Trevor Mendel J., Patton D. R., Ellison S. L., McConnachie A. W., 2011, ApJS, 196, 20
Simon J. D., Bolatto A. D., Leroy A., Blitz L., Gates E. L., 2005, ApJ, 621, 757
Stinson G. S., Brook C., Macciò A. V., Wadsley J., Quinn T. R., Couchman H. M. P., 2013, MNRAS, 428, 129
Swaters R. A., Sancisi R., van Albada T. S., van der Hulst J. M., 2009, A&A, 493, 871
Teyssier R., Pontzen A., Dubois Y., Read J. I., 2013, MNRAS, 429, 3068
Tolstoy E., Hill V., Tosi M., 2009, ARA&A, 47, 371
Tonini C., Lapi A., Shankar F., Salucci P., 2006, ApJ, 638, L13
van Zee L., 2001, AJ, 121, 2003
Verheijen M., de Blok E., 1999, Ap&SS, 269, 673
Vogelsberger M., Zavala J., Simpson C., Jenkins A., 2014, MNRAS, 444, 3684
Weinberg D. H., Bullock J. S., Governato F., Kuzio de Naray R., Peter A. H. G., 2015, Proc. Natl. Acad. Sci., 112, 12249
Weldrake D. T. F., de Blok W. J. G., Walter F., 2003, MNRAS, 340, 12
White S. D. M., Negroponte J., 1982, MNRAS, 201, 401
Yegorova I. A., Salucci P., 2007, MNRAS, 377, 507
Yoshino A., Yamauchi C., 2015, MNRAS, 446, 3749
Zavala J., Jing Y. P., Faltenbacher A., Yepes G., Hoffman Y., Gottlöber S., Catinella B., 2009, ApJ, 700, 1779

SUPPORTING INFORMATION

Supplementary data are available at *MNRAS* online.

Galaxy_RCs.txt

Please note: Oxford University Press is not responsible for the content or functionality of any supporting materials supplied by the authors. Any queries (other than missing material) should be directed to the corresponding author for the article.

APPENDIX A: SAMPLE OF ROTATION CURVES

In Fig. A1, we show the RCs of all observed galaxies used in our analyses, i.e. the same galaxies as appear in Table 1. We note that RCs of UGC1501, UGC5427, UGC8837, UGC5272, IC10, KK149 and UGC3476a are not extended to 3.2 R_D (the vertical dashed grey line of Fig. A1 indicates the position of 3.2 R_D for each galaxy), therefore, in order to know the value of the circular velocity at these radii we made extrapolations.

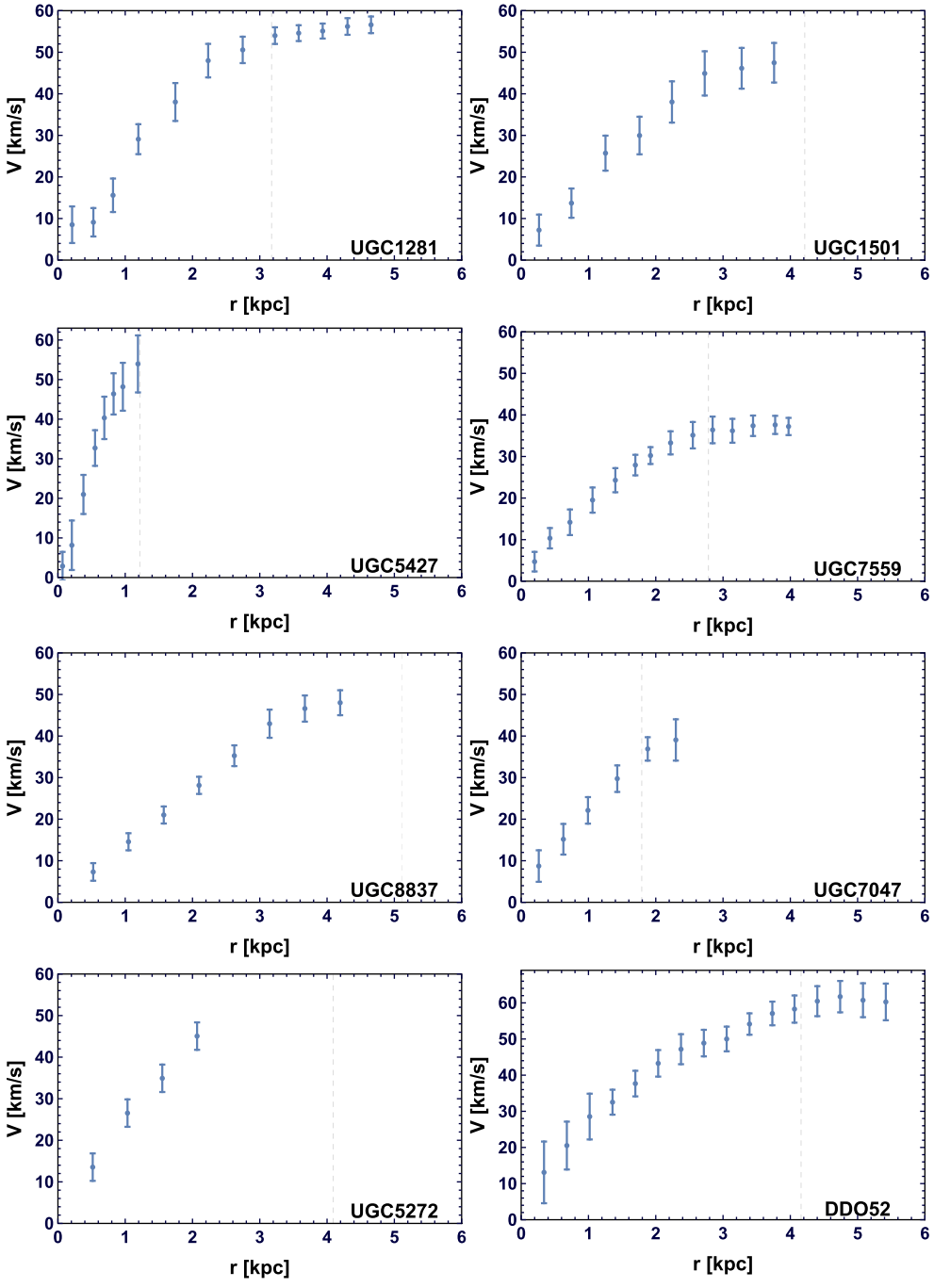

Figure A1. Individual RCs. Here, the R_{opt} are indicated by dashed vertical lines.

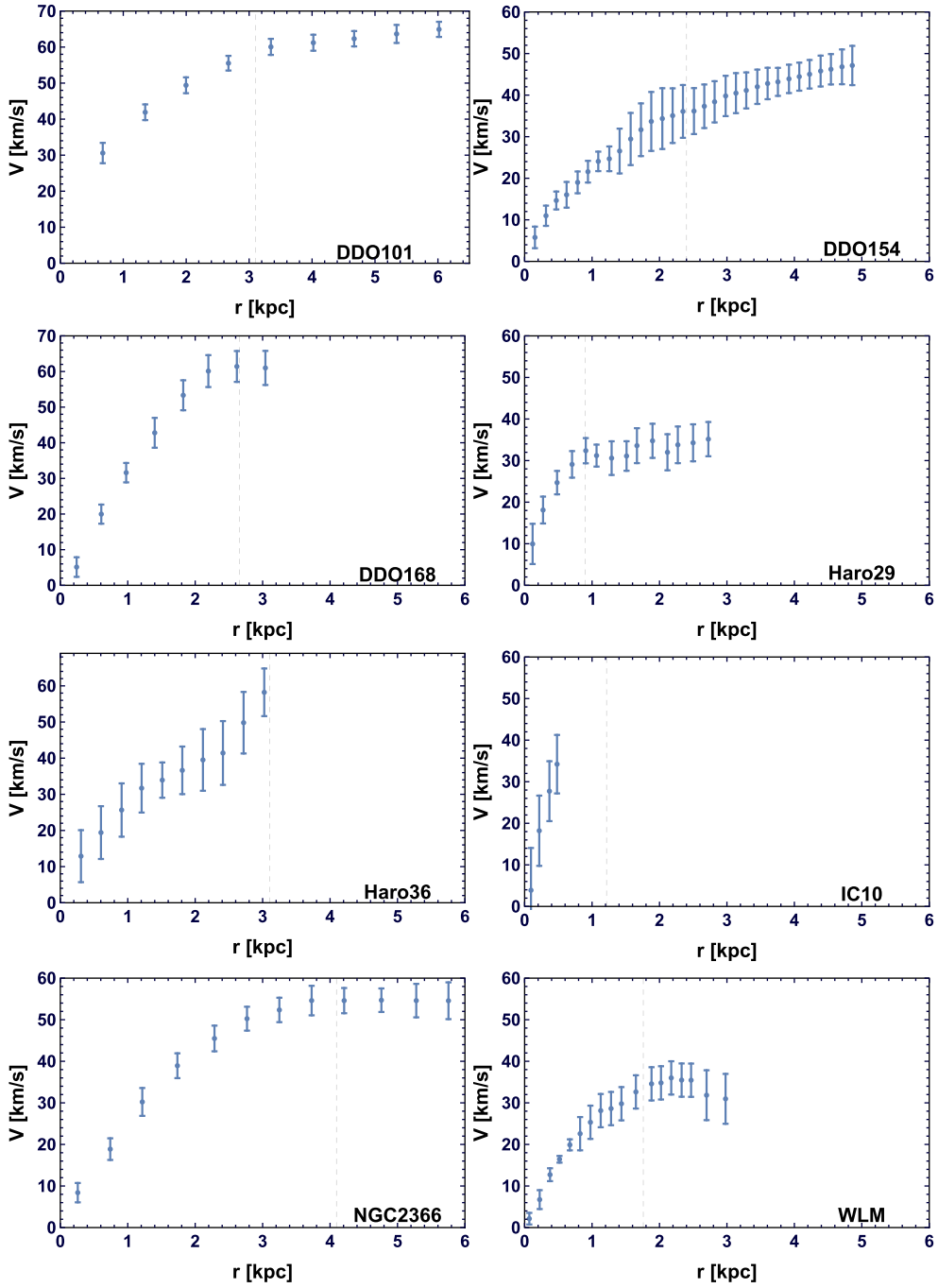

Figure A1 – *continued*

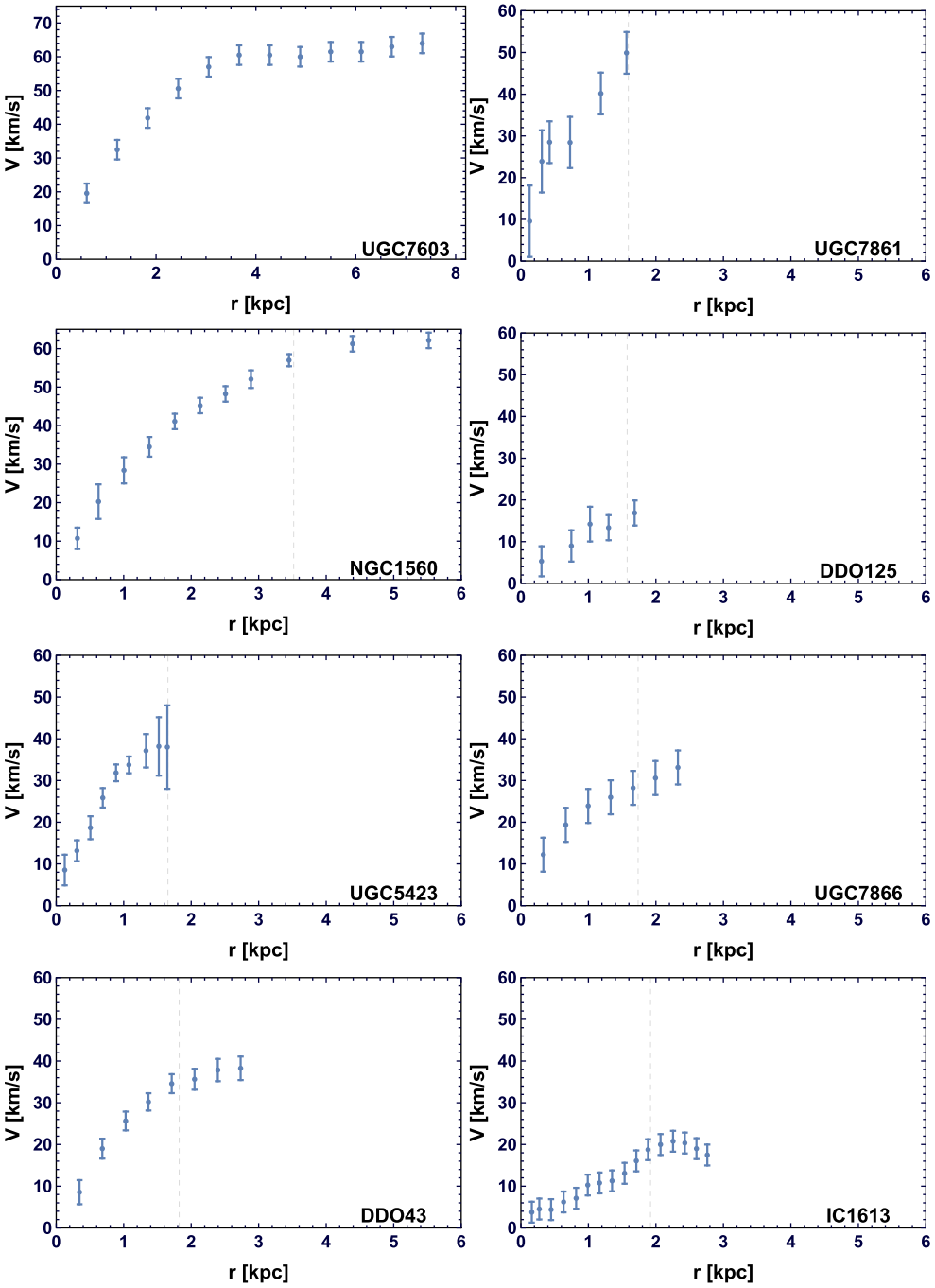

Figure A1 – *continued*

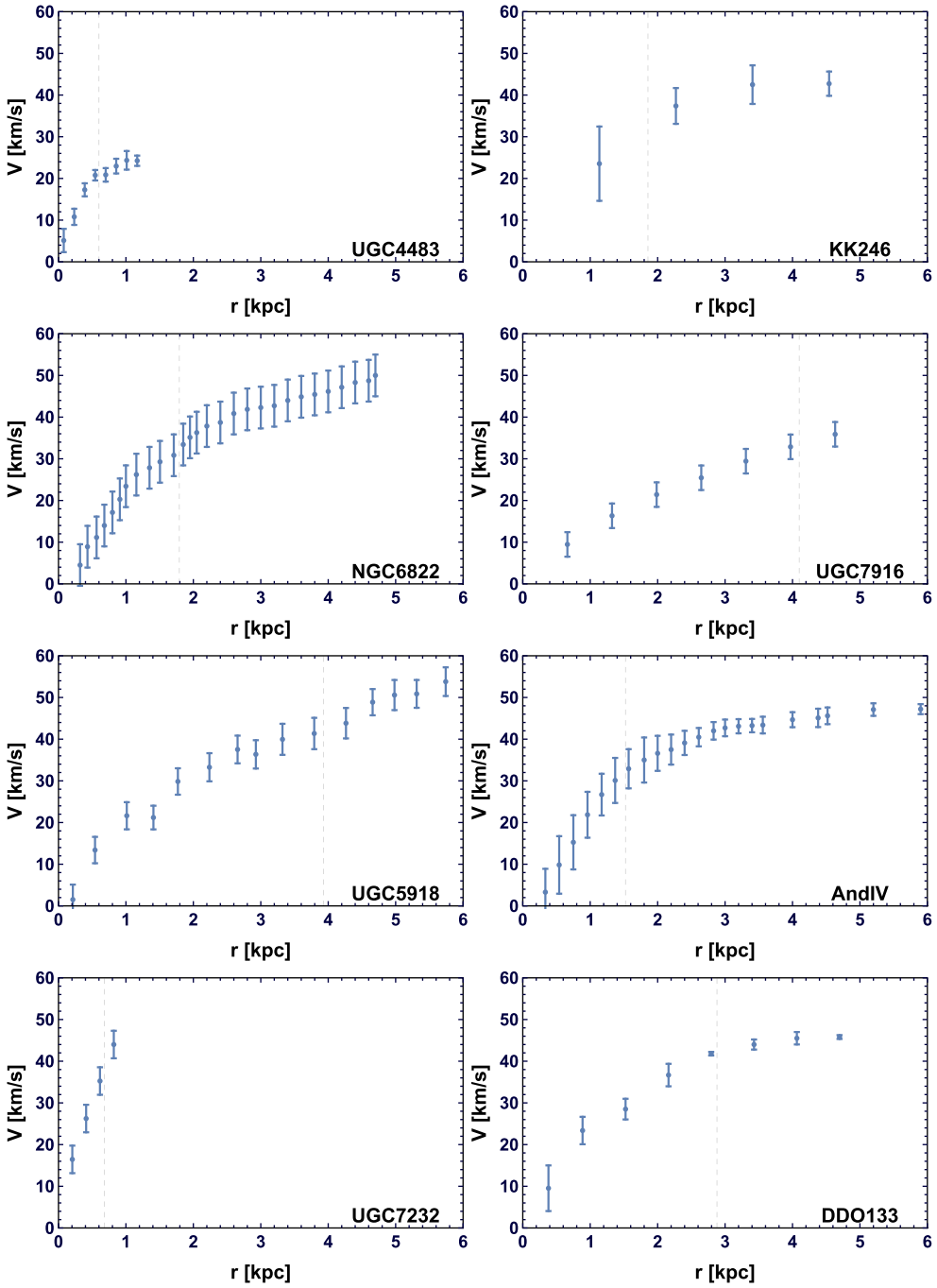

Figure A1 – *continued*

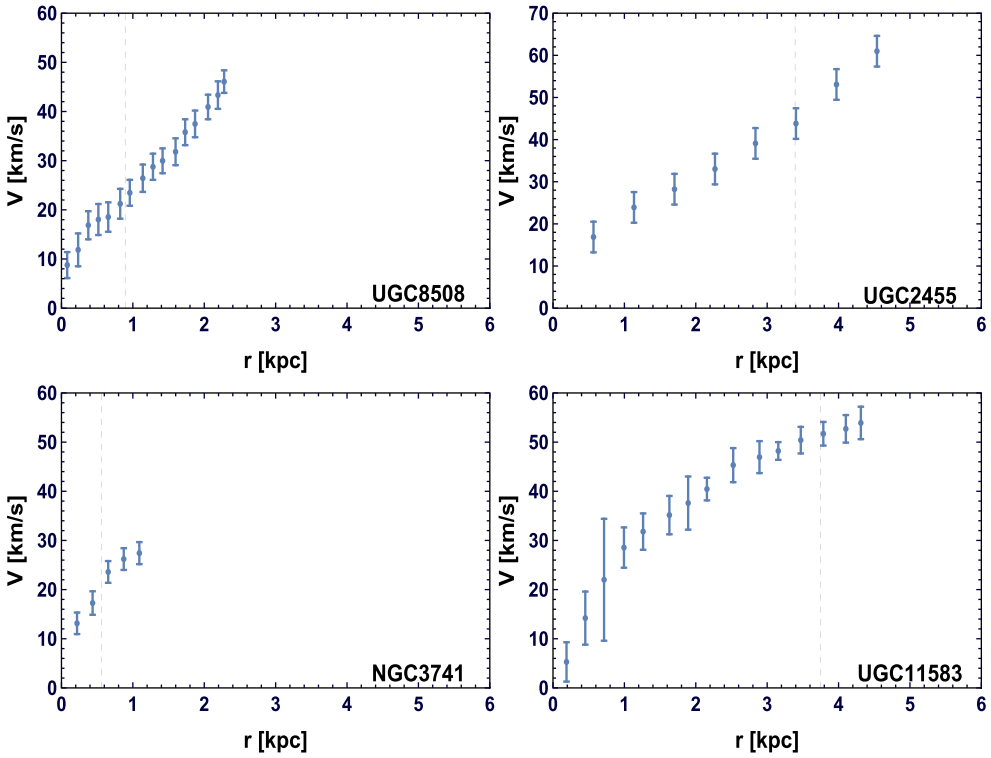

Figure A1 – *continued*

APPENDIX B: COMPARISON OF THE 'DD'URC AND THE URC OF PSS

In the left-hand panel of Fig. B1, as already discussed in Section 3, we plot our co-added double normalized RC (black stars) alongside with that of the PSS four luminosity bins. In this figure, the joined red dots correspond to the first luminosity bin, the joined green squares correspond to the sixth luminosity bin, the joined orange diamonds to the ninth luminosity bin and the joined pink triangles correspond to the 11th luminosity bin with inside 40, 70, 40 and 16 normal spirals, respectively (see fig. A1 of PSS). We realize that the co-added RC of the first PSS bin and synthetic dd RC have very similar profiles. However, the 'dd'URC appears to be slightly less concentrated than that of the first luminosity bin of PSS. The latter might indicate the continuation of the trend found in PSS, which states that the shape of RCs changes with luminosity. Therefore, in order to check whether we have this trend inside our sample we divided it in three subsamples in the following way: the most luminous, least luminous and the middle half. Then, we binned radially each subsample in the same way as described in Section 3. The data in the radial bins of each subsample are presented in Table B1. Furthermore, in the right-hand panel of Fig. B1, we compare the synthetic RC of the whole dd sample with three synthetic RCs of the above defined subsamples. All four RCs agree within their uncertainties and we do not find any trend of the shape of the RCs with luminosity. However, a weak trend is impossible to reveal. In fact the small number of galaxies in each bin induces some shot noise. Therefore, in order to further investigate this we need twice as many objects.

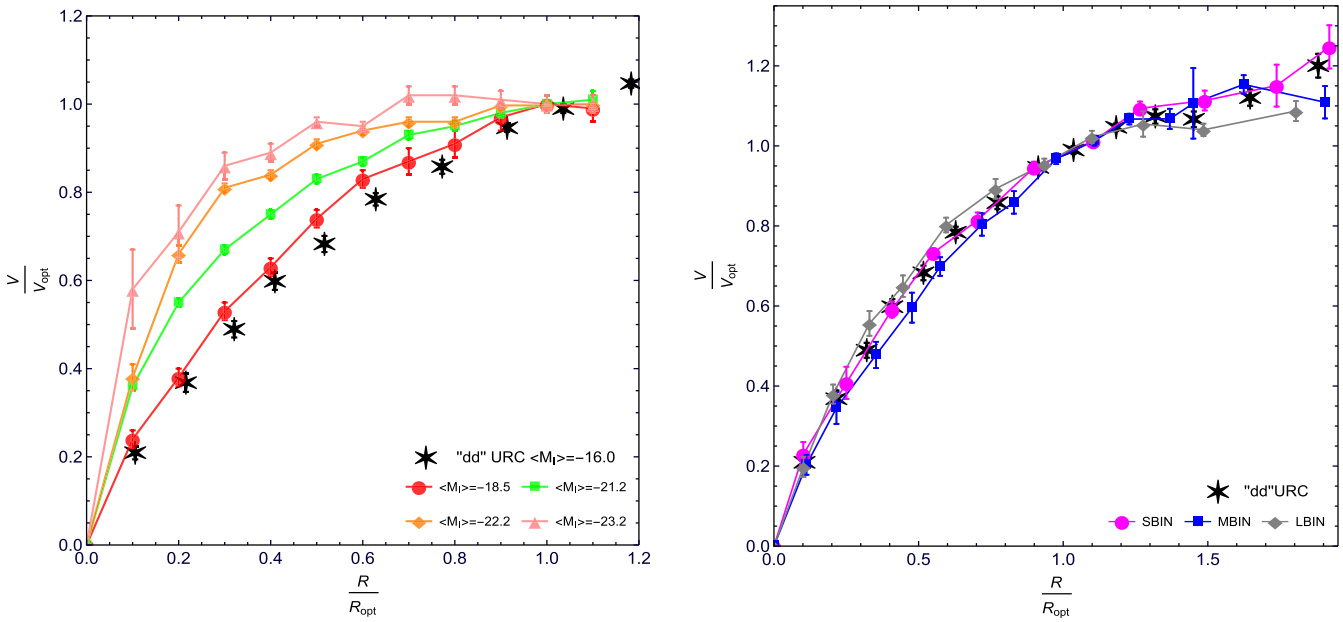

Figure B1. Left-hand panel: joined curves indicate the URC in normalized units of four luminosity bins of PSS. Right-hand panel: the URC in normalized units of three subsamples of dd galaxies (SBIN – smallest bin; MBIN – mean bin; LBIN – largest bin). Black stars indicate the synthetic RC of the whole sample of dwarfs disc galaxies.

Table B1. Data in the radial bins of three subsamples, ordered from least to most luminous. Columns: (1) bin number; (2) number of data points; (3) the central value of a bin; (4) the average co-added weighted normalized rotation velocity; (5) rms on the average co-added rotation velocity.

i	N	r_i	v_i	$\mathrm{d}v_i$	N	r_i	v_i	$\mathrm{d}v_i$	N	r_i	v_i	$\mathrm{d}v_i$
(1)	(2)	(3)	(4)	(5)	(2)	(3)	(4)	(5)	(2)	(3)	(4)	(5)
1	9	0.10	0.23	0.030	11	0.11	0.20	0.025	11	0.10	0.20	0.025
2	11	0.25	0.41	0.040	10	0.22	0.35	0.040	12	0.21	0.38	0.024
3	11	0.41	0.59	0.020	12	0.35	0.48	0.033	12	0.33	0.56	0.031
4	8	0.55	0.73	0.011	18	0.51	0.64	0.027	17	0.48	0.70	0.022
5	16	0.70	0.81	0.002	18	0.72	0.79	0.024	16	0.69	0.86	0.021
6	12	0.90	0.95	0.014	14	0.93	0.94	0.018	16	0.89	0.95	0.014
7	13	1.10	1.01	0.012	13	1.11	1.02	0.013	10	1.08	1.01	0.015
8	8	1.27	1.09	0.017	5	1.43	1.07	0.018	9	1.28	1.06	0.032
9	12	1.49	1.11	0.024	5	1.62	1.08	0.052	7	1.49	1.04	0.015
10	7	1.73	1.15	0.052	2	1.79	1.23	0.012	7	1.80	1.09	0.025
11	6	1.92	1.23	0.056	–	–	–	–	–	–	–	–

This paper has been typeset from a TEX/LATEX file prepared by the author.